Title

Hyperpolarized NMR study of the impact of alzheimer's disease on diabetes using a novel rat model

Journal

Journal of Physiology and Biochemistry, 82(1)

ISSN

1138-7548

Authors

Rehman, Usman

Datta, Keshav

Liu, Shie-Chau

et al.

Publication Date

2026-09-01

DOI

10.1007/s13105-026-01231-w

Hyperpolarized NMR Study of the Impact of Alzheimer's Disease on Diabetes Using a Novel Rat Model

[1]Usman Rehman, [2]Keshav Datta, [2]Shie-Chau Liu, [3]Jae Mo Park, [4]Renuka Sriram, [4]Donghyun Hong, [5]Qian Chen, [5]Hidetoshi Mori, [6]Vu Trinh, [7]Robert Berman, [2]Ralph Hurd, [2]Daniel Spielman, [1]Thomas Jue

[1]Department of Biochemistry and Molecular Medicine, University of California Davis, 4323 Tupper Hall, Davis, CA 95616, USA; [2]Department of Radiology, Stanford University, 1201 Welch Rd., Stanford, CA 94305, USA; [3]Advanced Imaging Research Center, University of Texas Southwestern Medical Center, 5323 Harry Hines Blvd., Dallas, TX 75390, USA; [4]Department of Radiology, University of California, San Francisco School of Medicine, USA; [5]Center for Genomic Pathology Laboratory, 4635 2nd Ave, University of California Davis, Room 3109, Sacramento, CA 95817, USA; [6]Department of Neurology, University of California Davis, 1515 Newton Court, Davis, CA 95616, USA. [7]Neurological Surgery, University of California Davis, 1515 Newton Court, Davis, CA 95616, USA.

ORCIDs:
Thomas Jue (0000-0003-1549-8414)

No. of Pages	25
Title Page	1
Abstract	1
Narrative	11
Table	6
Acknowledgments	1
Figure Captions	3
Declaration	1
References	5
Figures	12
Narrative Word count	6622

Running Title: Alzheimer's Disease and Diabetes

Correspondence:
Dr. Thomas Jue
Biochemistry and Molecular Medicine
University of California Davis
Davis, CA 95616-8635
Phone: (530) 752-4569
FAX: (530) 752-3516
E-mail: tjue@ucdavis.edu

Abstract

Most researchers have long focused on linkage between type 2 diabetes (T2D) and the increased risk of Alzheimer's disease (AD) but have often overlooked whether AD modulates T2D. Investigating the reciprocal interaction between two complex diseases provides perspectives on the mechanistic linkage. The endeavor, however, confronts challenges without a robust rodent model that develops T2D and AD as the animal ages. Cross breeding a T2D rat with a hemizygous TgF344AD +/- rat that contains the mutant human amyloid precursor protein (APPsw) and the presenilin 1 (PS1ΔE9) genes has produced a new T2D-AD +/- rat model. The T2D-AD +/- rat expresses both the T2D and AD phenotypes as the animal ages. As AD progresses, the time to T2D onset decreases, and the diabetes severity increases. Hyperpolarized NMR experiments using dynamic nuclear polarization (DNP) show that T2D and T2D-AD rats share a common metabolic impairment in the brain pyruvate dehydrogenase (PDH) activity as reflected in the NMR determined decline in the bicarbonate/lactate (bic/lac) ratio. The bic/lac ratio decreases in both T2D and T2D-AD brain. AD exacerbates the decline of the bic/lac ratio.

Keywords: Diabetes, Alzheimer's Disease, Dementia, Brain, Metabolism, NMR, Hyperpolarized NMR, Dynamic Nuclear Polarization, Pyruvate Dehydrogenase.

Abbreviations: T2D, type 2 diabetes; AD, Alzheimer's disease; EDTA, ethylenediaminetetraacetic acid; DNP, dynamic nuclear polarization.

INTRODUCTION

Many epidemiological studies have shown that type 2 diabetes (T2D) increases the risk of Alzheimer's disease (AD) [1-6]. Such an overlay of insulin insensitivity on AD poses a fundamental physiology question, since T2D typically involves the pancreas, liver, and muscle [7]. Even though the brain has insulin receptors and insulin can cross the blood brain barrier, the metabolic impact of insulin resistance on brain metabolism and AD pathogenesis defies any easy explanation [8-13]. The focus on the unidirectional impact of T2D on AD overlooks the reciprocal interaction of AD on T2D, which underscores the complex physiological interaction between T2D and AD. Indeed, studies on transgenic AD mouse models have shown that AD can promote hyperglycemia, a characteristic sign of diabetes [14, 15].

To better understand the metabolism dysregulation of T2D and T2D linked AD (T2D-AD) requires the aid of a convenient model that exhibits T2D and AD as the animal ages. Although rodents do not spontaneously develop AD, researchers have created an AD rat model by microinjecting into the egg an amyloid precursor protein (APP) and a human presenilin 1 (PS1) gene [16-18]. The resultant transgenic, hemizygous Fischer rat (TgF344AD +/-) expresses APP and PS1, shows neuronal loss, produces soluble Aβ oligomers, and shows cognitive impairment [19, 20]. It tracks the human inflammatory pathology more accurately than the corresponding mouse model and recapitulates the progressive sequence of human AD pathology [19, 21-24]. The TgF333AD +/- rats develop AD after 16 mos of age [19].

Cross breeding a TgF344AD +/- rat with the UCD_T2DM rat model has created a new T2D-AD +/- rat [25]. The UCD_T2DM rat model derives from the cross breeding of an obese Sprague Dawley (OSD) rat with a Zucker Diabetic Fatty (ZDF) rat to produce an offspring that displays as the animal ages adult-onset obesity, insulin resistance in the pre-diabetic state, which progresses to overt diabetes with ß-cell dysfunction, and fasting as well as non-fasting hyperglycemia. The animal, however, retains leptin signaling. The T2D progression parallels the one observed in humans. For the T2D-AD -/- and T2D-AD +/- rats, the body weight measurement, glucose assay, and insulin measurement affirm that they exhibit the T2D phenotype [19, 25]. In addition, the T2D-AD +/- rats expresses the AD transgenes as genotype analysis confirms, exhibits amyloid plaque by 9 mos of age, and performs very poorly on cognitive tests. A subsequent report will detail how T2D impacts AD. The current study examines how AD affects T2D.

With the growing presence of AD, the time to T2D onset decreases, while the T2D severity increases. The reciprocal interaction suggests that AD and T2D share a common metabolic dysregulation. In the brain, dynamic nuclear polarization (DNP) NMR experiments using [1-^{13}C]-pyruvate (pyr) precursor have mapped the metabolism in the Control (CRL), T2D-AD -/-, and T2D-AD +/- rats and have shown a common metabolic impairment in the pyruvate dehydrogenase (PDH) activity [26, 27]. Relative to control metabolism, the presence of T2D decreases markedly the PDH activity as reflected in the bicarbonate (bic) to lactate (lac) ratio. With AD in the T2D-AD +/- rat, PDH activity decreases further. The NMR experiments identify PDH as a common source of glucose oxidation impairment in both the T2D and T2D-AD brain [28-30].

As AD progresses, the increasing Abeta (Aβ) that characterizes AD progression also appears in the circulatory system. Aβ in the peripheral system can accelerate T2D onset/progression. Adding Abeta (Aβ) 1-40 to the isolated mitochondria from the spontaneously diabetic Goto-Kakizaki (GK) rat depresses oxidative phosphorylation [31]. Studies have also shown that amyloid deposit, often termed islet amyloid pancreatic peptide (IAPP), appears in the β pancreatic islet as a hallmark of T2D. Indeed, IAPP damages the insulin producing cells to induce hyperglycemia [32].

Although the precise mechanism affecting the reciprocal interaction of AD and T2D remains presently uncertain, the T2D-AD +/- rat model will facilitate researchers' effort to clarify the underlying mechanism linking AD and T2D, especially as it pertains to peripheral role of Aβ.

MATERIALS AND METHODS

ANIMAL MODEL

Animals

Cross breeding a T2D rat with a hemizygous TgF344AD +/- rat containing "Swedish" mutant human APP (APPsw), PS1 (human presenilin-1 with mutant exon 9, PS1ΔE9), and the mouse prion promoter (mPrnp) produced in filial generation 9 the colony founders that expressed the transgenes and exhibited a non-fasting plasma glucose level greater than 250 mg/dL at 3 months of age, the T2D-AD +/- rat model [19, 25, 33]. The T2D-AD -/- rat displayed only the T2D phenotype.

The T2D-AD -/-, and the T2D-AD +/- rats were bred, housed, and maintained at the UC Davis Animal Facility in Meyer Hall. Because the AD transgenes appeared only in one chromosome, the (+/-) designation denoted the hemizygosity. The symbol -/- indicated the absence of the AD transgenes. Because the T2D-AD rats derived from a Sprague-Dawley (SD) rat line, a SD rat served as the control.

All experiments were conducted in compliance with protocols approved by the Institutional Animal Care and Use Committee (IACUC). Because the male and female rats did not share identical obesity, weight, and diabetes incidence profiles, the initial study focused on male rats.

DNA Extraction and Genotyping

A 2-mm ear punch tissue was collected from three-week-old rodents using a hand-held ear punch tool (Fine Science Tools, Heidelberg, Germany). The tissue DNA was extracted using the AccuStart^{TM} II Mouse Genotyping Kit (Quantabio, Beverly, Massachusetts). The DNA was either stored at -20°C or kept on ice and used in the polymerase chain reaction (PCR).

The genotyping procedure used the ear tissue extract and followed a modified protocol 699 from the Rat Regional Resource Center (RRRC) at the University of Missouri to confirm the AD transgene integration. The AD transgenes originated from the TgF344-AD +/- rat model, which was derived from a Fischer 344 (F344) rat co-injected with APP_{sw} and PS1ΔE9 genes[19]. The amyloid beta (Aβ) precursor protein (hAPP) gene with the Swedish mutation (K595N/M596L) was driven by mPrp. The PS1ΔE9 gene was also driven by mPrp[19, 33]. Cergentis (Utrecht, Netherlands) confirmed the two transgenes integrated at the identical genome site in the TgF344AD_+/- and the T2D-AD +/- rats (data not shown).

Genotyping used 4 primers: 1) mPrp F sequence: 5'-CCT CTT TGT GAC TAT GTG GAC TGA TGT CGG-3' 2) mPrp R sequence: 5'-GTG GAT ACC CCC TCC CCC AGC CTA GAC C-3' 3) APP F sequence: 5'-CCG AGA TCT CTG AAG TGA AGA TGG ATG-3'4) PS1 F sequence: 5'-CAG GTG GTG GAG CAA GAT G-3' (Integrated DNA Technologies, Coralville, IA). Working solutions of 10 µM primer were formed by diluting the 100 µM stock primer solution in nuclease-free water. Solutions were stored at -20°C.

Polymerase Chain Reaction (PCR)

Sterile RNase- and DNase-free filter pipette tips were used in the PCR and other steps. The 2X Taq PCR Master Mix with dye (APExBIO, Houston, TX) contained all PCR components, except the primers, and template DNA. DNA samples were diluted 1:100 in 10 mM Tris/0.1 mM EDTA pH 8.0. PCR components were mixed in 0.2 mL PCR tubes. One PCR reaction mix contained 12.5 µL of 2X Taq PCR Master Mix with dye; 0.5 µL of 10 mM mPrp F, mPrp R, APP F, and PS1 F; 9.5 µL of nuclease-free water (Biologix USA, Camarillo, CA); and 1 µL of 1:100 diluted DNA. The PCR reactions used a GeneAmp® PCR System 9700 (Applied Biosystems, Foster City, CA) and followed the cycle parameters: (a) 94°C for 2 min, (b) 94°C for 30 s, (c) 55°C for 30 s, (d) 68°C for 1 min, (e) repeat steps (a)-(d) 29 times for 30 cycles total, (f) 68°C for 5 min, and (g) 4°C hold.

Gel Electrophoresis

The 5X Tris-borate-EDTA (TBE) buffer was prepared by dissolving 54 g of Tris, 27.5 g of boric acid, and 4.65 g of Na^+-EDTA dihydrate into 800 mL of Millipore water, which was brought up to 1L. Aliquots of 5X TBE buffer were mixed with an appropriate amount of Millipore water to make 1X TBE buffer. Dissolving 1 g of low electroendosmosis (EEO) agarose (Genesse Scientific, El Cajon, CA) and 10 mL of 5X TBE buffer into 39 mL of Millipore water formed a 2% TBE gel. The mixture was heated until the agarose dissolved. Once the solution became clear, 2.5 μL of ethidium bromide (Sigma-Alrich, St. Louis, MO) was added. The mixture was poured into a 7 × 8 cm DNA Plus Mini Agarose Gel System (USA Scientific, Ocala, FL). Two 10-well combs were inserted and removed after the gel had solidified 60 min later. The gel tank was filled with 350 mL of 1x TBE buffer.

To create the DNA ladder, 5 μL of a standard (PureView^{TM}) with 50-1,500 base-pairs (Azura Genomics, Raynham, MA) was added to the first gel well. 10-15 μL of PCR reaction samples were added into the remaining wells. The electrophoresis ran at 70 volts for 45 min. An FBTI-614 Ultra-Violet (UV) Transilluminator (Fisher Scientific, Waltham, MA) enabled the visualization of the gel bands. Lanes were analyzed for the appearance of APP, Prp, and PS1 bands at 400, 799, 1,300 bp, respectively.

HISTOLOGY

Amyloid

Rat brains were rapidly isolated and bisected into hemispheres. One hemisphere was fixed in 4% paraformaldehyde (PFA) before routine processing and paraffin embedding for histochemical analyses. The remaining hemisphere was weighed, snap frozen, and homogenized in 2 mL of ice-cold lysis buffer (Cell Signaling Technology Danvers, MA) supplemented with 1 mM phenylmethylsulfonyl fluoride for biochemical analyses.

Tissues were fixed in 10% neutral buffered formalin at room temperature for 24 h, then placed in 70% ethanol until processing, which was normally within 24 h. A Tissue-Tek VIP auto-processor (Sakura, Torrance, CA) was used to process tissues that were then embedded in Paraplast (melting temperature 56–60°C), sectioned to 4 μm, and mounted on glass slides. Tissues were further processed in a tissue cassette starting with 70% alcohol for 2 h, then transferred to 100% alcohol for another 2 h.

Antigen retrieval was performed for 20 min with formic acid (88-91%). Slides were blocked with normal goat serum, then incubated with a rabbit monoclonal anti-beta-amyloid, 17-24 antibody (Clone [4G8], Catalog number 800701) overnight at room temperature in a humidified chamber, followed by a biotinylated goat anti-mouse secondary antibody (1:1000). The Vectastain ABC Elite Kit and a Diaminobenzidine Peroxidase Substate Kit (Vector Labs, Burlingame, CA) were used for amplification and visualization of signals, respectively [34]. ImageJ (NIH) analyzed quantitatively the digitized micrographs to determine the distribution of amyloid in different brain regions.

COGNITIVE PERFORMANCE TEST

Barnes Maze Description

The Barnes maze tested the hippocampal-dependent spatial learning and memory of rat subjects. A previous study utilized it to test the cognitive performance of the TgF344-AD +/- rat with the AD transgenes [19]. The Barnes maze comprised of a black circular platform, 165 cm in diameter, mounted on a rotating pedestal, 118.9 cm over the ground. Along the periphery were 20 evenly spaced holes, each 11.5 cm in diameter. The holes were separated from each other by 11 cm and were 5 cm from the maze edge. One hole led to a dark, recessed chamber (escape box). The remaining 19 holes led directly to the ground.

A black box was used to cover the rat in the maze center at the beginning of the trial. On the ceiling were bright overhead lights, which could be turned on and off via a switch. On the side of the

ceiling were switch-controlled side lights. The maze was separated from the computer and testers by a black curtain.

On test days, all three walls surrounding the maze contained white cardboard cue cards. Specifically, the wall facing the black curtain contained a square. The wall to the left of the curtain contained a T-shaped picture, and the wall to the right of the curtain contained a sideways hourglass picture. A video camera (Polestar II EQ610, EverFocus Electronics, New Taipei City, Taiwan) was suspended 144.4 cm above the maze. A desktop computer located near the testers, beyond the black curtain, contained the EthoVision (Noldus, the Netherlands) software, which recorded rat movement via the camera.

Barnes Maze Habituation

Three days prior to the Barnes maze test, experimenters handled each rat for 10 min every day to familiarize the animal with human touch. On day 1, rats in a cage were brought into the testing room. The cages were placed on a side table for 5 min to allow the rats to acclimate. Each rat was then placed on the maze in ambient light for 10 min. The maze had no escape box, and the wall had no cue cards. The rat was allowed to freely explore the maze. If the rat fell off the maze, it was placed back onto the maze and allowed to complete its 10 min exploration. After the exploration period, the rat was returned to its cage. The maze was immediately cleaned with 10% chlorhexidine diacetate (Nolvasan), before the next rat was placed on the maze.

Barnes Maze Behavioral Testing

The testing started on day 2 and lasted until day 6. At the beginning, rats in their cage were brought to the testing room and acclimated for 5 mins. The escape box was placed under 1 hole, and cue cards were placed on the appropriate walls. A rat was placed onto the center of the maze, where it was promptly covered by a black Plexiglas box. No light could penetrate the box. The rat remained there for the initial period of 60 sec. During this period, bright overhead lights were turned on, and white noise was activated. After the initial period, the box was raised by one experimenter, who reached in from beyond the curtain to remove the box. He/she promptly stepped behind the closed curtain around the test area. A second experimenter immediately clicked the “Record” button on the EthoVision software. All experimenters remained silent in the room during the trial. The rat had 90 sec to find the escape hole.

If the rat did not find the escape hole in 90 sec, the experimenter led the rat to the escape box where it stayed for 15 sec. Whether the rat found the escape box on its own or was guided to the escape box, each rat remained in the escape box for 15 s at the end trial period. While the rat was in the escape box, the bright overhead lights were turned off, and the white noise machine was inactivated. A second trial then started with the same protocol. If the rat fell off the platform, the trial was terminated. The rat was still led to the escape box, before another trial started. This procedure was repeated 3 times for a total of 4 trials per rat per day.

Before the testing of each rat, the maze was cleaned with 10% Nolvasan to remove any olfactory cues from the previous rat. Singly housed rats were returned to their home cage after the trials. The same procedure was performed on days 2-6.

Barnes Maze Analysis

The escape latencies (time for the rat to enter the escape box) of the T2D-AD rats were analyzed for all trial days using Excel (Microsoft, Redmond, WA, USA). The analysis of the video recording quantified the search strategies: direct, serial, and random. These strategies evaluated spatial memory and cognitive ability[35]. Search strategies fell into 3 categories: 1) random: animals moved across the platform in no detectable pattern; 2) serial: animals sequentially checked openings at the periphery of the maze; and 3) direct: animals moved directly to the escape box or traveled to the hole adjacent the

escape box, then to the escape box. A chi-square analysis after collapsing data across all trials evaluated the distribution of the search patterns [35, 36]

METABOLIC AND PHYSIOLOGICAL PROFILE

Fasting Glucose

Rats were fasted for up to 14 h overnight and 300 μL of fasting blood was collected from tail tips of non-anesthetized rats into Microvette® CB 300 blood collection tubes with potassium-EDTA (Sarstedt, Nümbrecht, Germany). Samples were kept on ice and centrifuged at 1,500 RCF and 4°C for 10 min. Plasma was stored at -80°C. Samples were thawed on ice for fasting glucose and insulin measurements. Glucose standards of 100, 200, 300, 400, and 500 mg/dL were prepared by dissolving β-D-glucose (ICN Biomedicals Inc., Aurora, OH) into appropriate amounts of water. Fasting glucose was measured using an enzymatic assay. 3 μL of a standard or plasma was mixed with 300 μL of Glucose Oxidase Liquid Reagents (Pointe Scientific, Canton, MI) and incubated at 37°C for 5 min. A VMax® Kinetic Microplate Reader (Molecular Devices, San Jose, CA) read at glucose output signal at 490 nm.

Non-Fasting Glucose

Rat tail tips were pricked with a lancet and 6 μL of whole blood was obtained. The non-fasting glucose was measured with a glucose test strip and a TD-4116 glucometer (Metene, Santa Clara, CA). Diabetes onset was assigned, when measured non-fasting blood glucose concentrations reached 250 mg/dL.

Insulin

Fasting insulin was measured using a rat/mouse insulin ELISA (EZRMI-13K) from Millipore Sigma (Burlington, MA) [37-39]. Sample insulin was added to plate-wells coated with monoclonal mouse anti-rat insulin antibodies. Biotinylated polyclonal antibodies were added to wells. Unbound material was washed away. Horseradish peroxidase was added to wells. Free enzyme conjugates were washed away. Quantification of antibody-enzyme conjugates was measured from the peroxidase activity with 3,3',5,5'-tetramethylbenzidine (TMB). A BioTek Synergy H1 Multimode Reader (Agilent Technologies, Santa Clara, CA) assessed the enzyme activity by measuring the absorbance at 450 nm corrected with the absorbance at 590 nm. The corrected 490 nm absorbance was directly proportional to sample insulin concentrations, which could be interpolated from a reference curve in the same assay with a known rat insulin standard.

HYPERPOLARIZED NMR

^{13}C Substrate Preparation

For each hyperpolarized experiment, 54 μL of 15.5 M [1-^{13}C] pyruvate (Sigma Aldrich) mixed with 15 mM trityl radical AH11141(GE Healthcare) was polarized between 3-4 hours in a SPINLab system (GE Healthcare) and dissolved using a 16 g solution of 40 mM tris (hydroxymethyl aminomethane), 100 mg/L ethylenediaminetetraacetic acid (EDTA), and 50 mM NaCl. The resulting 125 mM pyruvate (pyr) solution was neutralized with 640 μL of 125 mM NaOH buffer. 2.5-3.0 mL of this solution, adjusted to maintain a dose of 1 mmol/kg body weight, was used in the experiments to acquire data in a clinical 3T PET/MR scanner (GE Healthcare).

Data Acquisition

The animals were anesthetized using 2–3% isoflurane in ~1.5 L/min oxygen and catheterized in tail vein for intravenous administration of the hyperpolarized substrate. At the start of the experiment, a sterile ophthalmic lubricant was applied to the eyes to prevent corneal drying. Throughout the session,

animal vital signs including respiration, heart rate, temperature, and oxygen saturation, were monitored and respiration was consistently maintained at ~60 breaths per minute by regulating the isoflurane level. A warm water blanket placed underneath the animal was used to regulate the body temperature.

A custom-built birdcage RF coil (inner diameter 95 mm) tuned to the ^{1}H resonance was used to excite and acquire proton MR images. A single-shot fast spin echo (FSE) sequence was first used to acquire 10 slices each in the axial, coronal and sagittal planes (TR/TE = 1492/38.6 ms; 5 mm slice thickness; 0.47 mm in-plane resolution) for localization. A dual-echo T_2-weighted FSE sequence (TR/TE1/TE2 = 5000/11.3/ 56.7 ms; 2 mm slice thickness; 0.25 mm in-plane resolution; 256x256 matrix size; 8 echo train length; 25 slices; 8 min 5 s scan time) in the axial plane was used to determine the slice placement in the center of the brain for ^{13}C MRS acquisition. The B_0 field was optimized with linear shim currents to be spatially homogeneous in the slice of interest by minimizing the linewidth of the unsuppressed water signal from a position-resolved proton spectroscopy sequence.

For the ^{13}C data acquisition, a custom-made ^{13}C surface coil (40 mm diameter) was used to acquire data from an axial slice at the center of the brain. An 8 M ^{13}C urea phantom placed on the head of the rat was used to calibrate the flip angle by adjusting the transmit gain to obtain maximum signal from the phantom for a 90°-flip angle. Hyperpolarized [1-^{13}C] pyruvate solution was injected at a rate of 0.25 mL/s into the animal through the tail vein catheter and the spectral data acquisition began at the start of injection. A slice-selective free induction decay (FID) pulse and acquire sequence (excitation bandwidth = 2.2 kHz, pulse width = 1.8 ms, slice thickness = 10 mm, receiver bandwidth = 5000 Hz, N = 2048, flip angle = 10°, TR = 3 s) centered at [1-^{13}C] pyruvate resonance was used to acquire the carbon spectrum every 3 s for a total of 4 min. scan time (80 temporal data frames).

Spectral reconstruction and metabolite analysis

Custom-developed signal processing scripts in MATLAB (MathWorks, MA, USA) were used for data processing and model fitting. The FID data were apodized with 5 Hz Gaussian line broadening, zero-filled by a factor of four, and fast Fourier transformed to obtain the spectra. Zero-order and first-order phase corrections were performed on the spectra, and the metabolite time courses were calculated by integrating the [1-^{13}C] pyruvate, [1-^{13}C] lactate, [1-^{13}C] alanine, and [1-^{13}C] bicarbonate peaks in absorption mode. The total carbon (tC) signal was derived by summing the area under peaks (AUP) over the interval in which the bicarbonate signal was detectable. The metabolite ratios of pyruvate/lactate, pyruvate/bicarbonate, and lactate/bicarbonate were then computed.

Statistical Analyses

Data were reported as means ± standard error of the mean (SEM). All statistical analyses were performed using Microsoft Excel (Microsoft, Redmond, WA). Graphs were generated with SigmaPlot 10 (Grafiti LLC, Palo Alto, CA). Differences were considered significant if the p-values were less than the alpha value of 0.05. The statistical analysis also used two-tailed Student's t-test with Bonferroni correction, ANOVA with Tukey correction, and a modified Kaplan-Meier survival analysis followed by a log-rank test[40, 41]. The Barnes maze search strategy analysis used a chi-square analysis on collapsed data across all trial days[35].

RESULTS

Agarose DNA gel electrophoresis following polymerase chain reaction assayed for the presence of PS1, Prp, and APP in the T2D-AD -/- and T2D-AD +/- brains, fig 1. The far-left lane contained the DNA ladder. All rats exhibited the Prp gene band at 799 bp. Only the T2D-AD +/- rats displayed the AD genes: PS1 and APP gene bands at 1,300 and 400 bp, respectively. The T2D -/- rat showed only the Prp band.

A histological assay showed the presence of Aβ plaque of 9 mos T2D-AD -/- and T2D-AD +/- brains, fig 2. The T2D-AD -/- brain had no Aβ plaques, while the T2D-AD +/- brain displayed a significant amount. Image J quantified the Aβ plaques, fig 3, and showed the Aβ plaque distributed in percent of positive plaque area as follows: hippocampus (3.81±0.16), thalamus (1.68±0.13), and cortex (0.21±0.04). The Aβ plaques located primarily in the hippocampus, table 1.

The escape latencies of the T2D-AD -/- (n = 18) and T2D-AD +/- (n = 18) in the Barnes Maze test differed dramatically, fig 4. Over the course of 6 days, the T2D-AD -/- rats displayed a decreasing escape latency. In contrast, the T2D-AD +/- rats showed no significant change in escape latency, table 2. A statistically significant difference in the latencies between T2D-AD -/- and T2D-AD +/- occurred on day 5 and 6.

Assessing the use of direct, random, and serial search strategies also revealed a marked difference in the T2D-AD -/- and T2D-AD +/- rats, fig 5 and table 3. The T2D-AD -/- rats used a direct strategy more than T2D-AD +/- rats. The T2D-AD +/- rats employed predominantly a random strategy. A chi-square analysis of the collapsed data across all trials revealed a significant difference in the distribution of search patterns between T2D-AD -/- and T2D-AD +/- rats.

No rat model used primarily the serial search strategy: T2D-AD -/- (day 2, 11%; day 6, 5%); T2D-AD +/- (day 2, 5%; day 6, 12%). However, the T2D-AD -/- rat increasingly used the direct strategy to find the escape hole: T2D-AD -/- (day 2, 2%; day 6, 42%). In contrast, the T2D-AD +/- rat never shifted significantly to the direct strategy (day 2, 5%; day 6, 12%). Instead, it relied almost exclusively on a random strategy.

From 1 to 9 mos of age, the T2D-AD -/- and the T2D-AD +/- rats the body weights ranged from 114 to 577 g, fig 6 and table 4. At 5 mos of age, the T2D-AD -/- and the T2D-AD +/- rats' weights began to deviate. The T2D-AD +/- rats weighed significantly less than the T2D-AD -/- rat.

A modified Kaplan-Meier survival analysis followed by a log-rank test indicated a significant difference in the diabetes incidence between T2D-AD -/- and T2D-AD +/- rats, fig 7. A non-fasting glucose level of >250 mg/dl marked the threshold of diabetes. T2D-AD -/- rats displayed the 50% time point for diabetes incidence at 137±5 days (n=78), while the T2D-AD +/- rats developed the corresponding time point at 101±3 days (n=102). T2D-AD +/- rats exhibit diabetes 36 days earlier for the T2D-AD -/- rats.

The non-fasting glucose profiles of the T2D-AD -/- (n=12-68) and T2D-AD +/- rats (n=12-91) referenced to the months before or after diabetes onset of the T2D-AD -/- rat showed the glucose level profile, fig 8 and table 5. After the T2D-AD -/- diabetes onset, the glucose level began to rise. The T2D-AD +/- rats exhibited a similar profile, but diabetes onset occurred 1 month earlier. Glucose level rose at onset and remained high. Linear regressions on the data at -1, 0, and 1 months show T2D-AD -/- and T2D-AD +/- that the T2D-AD +/- rat non-fasting glucose level increased 1.6 times faster than the corresponding glucose level in the T2D-AD +/- rat.

The fasting glucose profiles for the T2D-AD -/- rats (n = 7-21) and T2D-AD +/- (n = 8-25) referenced to the months before or after diabetes onset of the T2D-AD -/- rat as 0 mos showed no significant glucose level change before diabetes onset, fig 9 and table 5. With the T2D-AD -/- rats, the glucose level did not change significantly until 2 mos after diabetes onset. For the T2D-AD +/- rats, glucose level increased 1 mo after diabetes onset. The T2D-AD +/- rat showed glucose rising 1.6 times faster than the T2D-AD -/- rat.

In the fasting insulin profiles, the T2D-AD -/- (n=4-10) and the T2D-AD +/- (n=3-10) rats referenced to the diabetes onset of the T2D-AD -/- rat at 0 mos differed significantly, fig 10 and table 5. For the T2D-AD -/- rat, insulin rose at diabetes onset to 3.84±0.42 ng/ml and remained at the same level for an additional month. 2 months after onset, the insulin began to crash. 4 months after onset insulin level reached to 0.73±0.18 ng/ml. In contrast, the T2D-AD +/- insulin reached its maximum level, 4.42 ng/ml at its diabetes onset. 1 month post onset, insulin dropped immediately to 1.66 ng/ml ±0.23. 4 months after onset, the insulin level crashed to 0.37 ng/ml ±0.13.

The 2 min averaged of the ^{13}C NMR signals revealed the metabolite distribution and enzyme kinetics in CRL (n = 3), T2D-AD -/- (n = 7), T2D-AD +/- (n = 8) brain, fig 11 and table 6. In comparison to the CRL rat and the total carbon signal (tC), lac/tC increased from 0.109±0.006 (CRL) to 0.146±0.008 (T2D-AD-/-) to 0.212±0.013 (T2D-AD +/-). Ala/tC also increased from 0.051±0.004 to 0.076±0.008 to 0.078±0.004. However, bic/tC decreased from 0.018±0.002 to 0.011±0.001 to 0.009±0.001. Relative to the CRL, the presence of T2D lac/tC increased by 34% and ala/tC by 49%. In the presence of T2D and AD, lac/tC increased by 94% and ala/tC increased by 53%. Bic decreased correspondingly from 0.018±0.002 to 0.011±0.001 to 0.009±0.001. Bic level dropped by 39% in T2D-AD -/- and by 50% in T2D-AD +/-.

In comparison to the control (CRL), bic/lac ratio decreased from 0.164±0.012 (CRL) to 0.075±0.005 (T2D-AD-/-) to 0.042±0.004 (T2D-AD +/- rat), fig 12. Relative to the CRL, the bic/lac ratio dropped 54% in T2D-AD -/- and 74% in T2D-AD +/-. T2D-AD +/- brain showed the most precipitous drop.

DISCUSSION

T2D with an AD Overlay

The T2D-AD +/- rat provides a unique model to interrogate the interaction T2D and AD. It expresses the APP and PS1 genes and displays the AD phenotype. Moreover, both the T2D-AD -/- and T2D-AD +/- rats show a progressive change in the diabetes as the animals age, consistent with previous reports [19, 25]. The T2D-AD -/- rat, however, does not spontaneously develop amyloid plaque and does not display any AD characteristics.

With the expression of the AD genes, the T2D-AD +/- shows an abundance of amyloid plaque at 9 mos of age. According to previous studies, the TgF344AD +/- the amyloid burden appears only after 16 mos of age [19]. The presence of T2D accelerates brain amyloid formation. In the presence of brain amyloid, the T2D-AD +/- rat exhibits an impaired cognitive ability. The escape latency of the T2D-AD -/- rat decreases from day 2 to day 6 in the Barnes maze trial (from 89 s to 74 s). In contrast, the T2D-AD +/- rat also shows no change in the escape latency and no detectable capacity to learn the maze. AD significantly impairs the cognitive ability of the T2D-AD +/- rat. In contrast, the T2D-AD -/- rat does not show any cognitive impairment.

Evaluating the three distinct escape strategies also reveals the AD-induced impairment. The random, serial, and direct strategies characterize the escape search as follows: 1) random: animals move back and forth across the platform with no discernible pattern toward the escape compartment, 2) serial: animals sequentially check each opening at the periphery of the maze to find the escape hole, and 3) direct: animals directly travel to the escape hole. Previous studies have used fractional changes in the direct strategy as cognitive performance assessments [35, 36]. Indeed, the contrasting escape search patterns of the T2D-AD -/- and the T2D-AD +/- rats support the escape latency analysis and confirm the AD induced cognitive impairment.

AD Impact on T2D

Studies usually focus on the impact of T2D on AD pathogenesis and have often overlooked the physiological impact of AD on T2D onset/progression. Indeed, the body weight profile hints that AD affects T2D. Both T2D-AD -/- and T2D-AD +/- rats have similar body weights until 5 mos of age. Between 6 and 9 mos of age, the T2D-AD +/- body weight falls significantly below the corresponding T2D-AD -/- body weight.

The diabetes incidence profile confirms that T2D-AD +/- rats exhibit an earlier diabetes onset than the T2D-AD -/- rats. Instead of 137 days in the T2D-AD -/- rats, the 50% diabetes incidence onset date decreases to 101 days in the T2D-AD +/- rat. The glucose profiles corroborate. With the non-fasting

glucose assay, the T2D-AD +/- rat displays a diabetes onset 1 month earlier than the T2D-AD -/- rat. With the fasting glucose profile, the T2D-AD +/- rats, glucose level has already risen 1 month before the onset of diabetes in the T2D-AD -/- rat. Moreover, the T2D-AD +/- glucose level rises more rapidly and maintains a level well above the corresponding glucose level in the T2D-AD -/- rat.

Analyzing the T2D-AD +/- and T2D-AD -/- insulin profile also reveals that AD accelerates the onset of diabetes. The T2D-AD +/- insulin peaks one month earlier than the T2D-AD -/- rat. One month after diabetes onset, T2D-AD +/- insulin level drops to 37% of the peak value. 2 months after diabetes onset, insulin drops to 15% of its peak value. In contrast, insulin level one month after diabetes onset does not change significantly in T2D-AD -/- rat. 2 months after diabetes onset, insulin decreases to less than 30% of its peak value. The T2D-AD +/- rat shows a much faster rise and fall of insulin than the T2D-AD -/- rat [25]. The diabetes incidence, glucose, and insulin profiles all point to AD accelerating diabetes onset/progression.

Previous studies have observed that AD induces glucose intolerance and have posited an amyloid linkage [14, 15, 42]. In T2D, the presence of IAPP, often termed amylin, damages the insulin producing cells in the pancreas [32]. Amylin, a 37 amino acid peptide, shares many pathological features with β-amyloids (Aβ) and facilitates amyloid formation in brain [43]. With the addition of Aβ 1-40 to isolated mitochondria of the spontaneously diabetic Goto-Kakizaki (GK) rat, oxidative phosphorylation decreases sharply [31]. The present study shows that the AD induced T2D extends well beyond glucose intolerance and affects the onset/progression of T2D. Although the precise mechanism affecting the reciprocal interaction of AD and insulin insensitivity remains presently uncertain, the T2D-AD +/- rat model will help researchers clarify the role by which AD exacerbates T2D, especially with respect to the role of peripheral Aβ.

T2D and AD Brain Metabolism

Insulin insensitivity stands as a central characteristic of T2D. How insulin insensitivity affects the brain remains unclear. Orthodox physiology focuses on the insulin action in pancreas, liver, muscle, and fat cells and asserts that the brain always takes a constant cut of the available glucose [13]. Consequently, insulin insensitivity should not have a prominent role controlling glucose or oxidative metabolism in brain.

Yet, insulin can cross the blood brain barrier, can penetrate the circumventricular organs, including the arcuate and ventromedial nuclei of the hypothalamus, and can enter the cerebrospinal fluid [8-12]. The brain has insulin receptors. Whether the T2D brain has an insufficient amount of insulin reaching the cerebrospinal fluid (CSF) or suffers from insulin resistance poses a critical question in physiology [2, 4, 5, 44, 45].

Studies have indicated that AD brain displays an altered metabolism, especially with respect to glucose oxidation [28, 46]. Although glucose delivery to the brain remains constant, insulin may still alter the metabolic pathways and diminish the available energy required for learning and memory formation [3, 4]. The simplistic approach in augmenting insulin through intranasal insulin or stimulating insulin with glucagon-like peptide-1 agonist (GLP-1), such as liraglutide, seems like an easy therapeutic approach to mitigate T2D-linked AD. However, studies have unsuccessfully shown that intranasal insulin improves AD memory function in patients [47, 48]. Other studies administering liraglutide, a (GLP-1) agonist that binds the GLP-1 receptor to stimulate insulin secretion has failed to show consistent efficacy [49-52].

AD can also impair glucose oxidation in the T2D brain arising from a deficient astrocyte to neuron lactate shuttle (ANLS). PET and functional magnetic resonance imaging (fMRI) observations have delineated metabolism in the astrocyte vs neuron to account for the observed ratio of the cerebral oxygen metabolism rate ($CMRO_2$) over the cerebral glucose metabolism rate (CMRglc), $CMRO_2$/CMRglc or OGI, which falls below its theoretical value of 6. Pellerin and Magistretti have proposed a model that compartmentalizes glycolysis primarily in the astrocytes, which uptake glucose and produce lactate [53, 54]. Astrocytes then release lactate as a fuel source for the neurons. Lactate provides the fuel for neuron oxidative phosphorylation, which couples directly with the glutamate neurotransmission cycle (V_{cycl})

between astrocytes and neurons [55]. After neuron firing, the glutamate in the postsynaptic cleft enters the astrocytes where it gets converted to glutamine for transport back to the neurons for the next V_{cycl}. A deficient ANLS coupling to V_{cycl} provides an explanation in of OGI discrepancy and suggests a mechanistic basis for how AD exacerbates the bioenergetics of the T2D brain.

DNP and Pyruvate Dehydrogenase Activity

Hyperpolarized DNP NMR experiments suggest a shared metabolic dysregulated pathway in T2D and the AD brain. Because of the enhanced sensitivity, DNP can observe the rapid enzymatic conversion of pyruvate to lactate, alanine, and bicarbonate. These conversions reflect the glycolytic activity in the cytosol of lactate dehydrogenase (LDH) and alanine transaminase (ALT), and the oxidative activity in the mitochondria of pyruvate dehydrogenase (PDH), which critically regulates the TCA cycle flux and oxidative phosphorylation. The reactions catalyzed by LDH and ALT form lac and ala, respectively, while the reaction catalyzed by PDH releases CO_2, which in the cell forms bicarbonate. Bic then reflects PDH activity, while lac and ala reflect primarily the LDH and ALT activities.

Relative to the CRL brain, bic formation in T2D-AD -/- and T2D-AD +/- brain decreases by 39% and 50%, respectively. A falling bic level reflects a declining PDH activity. T2D inhibits PDH activity. T2D in the presence of AD inhibits PDH even further. A decreased PDH activity suggests an impaired oxidative phosphorylation. Given the decreased PDH activity, the rising pyruvate pool should then enhance lac and ala formation. Indeed, relative to the CRL brain, T2D-AD -/- and T2D-AD +/- brains produce 34% and 94%, respectively, more lactate/tC than the control brain. In the case of ALT activity, T2D-AD -/- and T2D-AD +/- brains also increase ala formation by 49% and 53%, respectively.

Indeed, the bic/lac metabolite ratio captures the distinct metabolism transition from CRL to T2D and T2D-AD. Relative to CRL, the bic/lac ratio in T2D-AD -/- brain decreases 54%. The ratio in T2D-AD +/- brain decreases 74%. Preliminary data indicate that bic/lac ratio in TgF344AD +/- brain, which only expresses the AD phenotype, decreases 46%. As such, the bic/lac ratio shows that T2D in the presence of AD will severely impair brain metabolism. Further studies must now clarify the regulatory mechanism and how to use the bic/lac ratio as a biomarker of T2D, AD, and T2D-AD.

Invoking an impaired ANLS to explain the observed PDH change provides one explanation. A competing glycogen sparing glucose (GSG) model provides a more satisfying explanation [56]. In the glycogen shunt model, the use of the astrocyte glycogen during neuron firing spares glucose for use in the neurons. Indeed, steady state ^{13}C MRS experiments with [1-^{13}C] glucose and [2-^{13}C] acetate have noted that elderly patients exhibit decreased V_{TCA} and V_{cycle} in the neurons [57]. ^{13}C NMR studies have already reported that insulin insensitivity in T2D decreases glycogen synthesis in human skeletal muscle [58]. Presumably the insulin insensitivity in T2D will also decrease the glycogen pool in brain. Indeed, studies have also shown that AD decreases glycogen synthase kinase (GSK) activity in brain. Consequently, the decreasing glycogen pool size in brain and muscle along with the GSG model provides a common mechanistic explanation of the complex interplay between AD and T2D.

Linking AD to Peripheral T2D Interaction

Researchers have postulated both an amyloid cascade and a mitochondria cascade theory to explain AD pathogenesis[59-61]. One posits amyloid plaque initiates AD, while the other focuses on mitochondria dysfunction as the primary driver. Studies have detected that insulin insensitivity indeed decreases glucose uptake in T2D brain and alters mitochondrial function, which then exacerbates neuroinflammation and promotes AD pathogenesis [62-65]. Moreover, amylin, a pancreatic β-cell hormone co-secreted with insulin forms pancreatic amyloid in T2D and synergistically interacts with brain amyloid β (Aβ) pathology in both sporadic and familial Alzheimer's disease (AD) [66]. How AD affects T2D, however, remains largely unexplored. Nevertheless, researchers have shown that Aβ 1-40 can impair mitochondria function in diabetes [31]. As AD progresses, the circulatory level of Aβ 1-40 does indeed increase [67]. Whether Aβ 1-40 or other Aβ fragments influences the course of diabetes poses a provocative question.

Conclusion

The development of the T2D-AD +/- rat model expressing APP and PS1 and T2D opens a unique opportunity to explore the interaction of AD on T2D onset/progression. AD accelerates the onset/progression of T2D. DNP NMR has observed that AD further depresses the T2D brain PDH activity as reflected in the bic/lac ratio. With AD, T2D the overall diabetes onset decreases, while its progression worsens. The present study has introduced a novel model and an experimental approach to better understand the biochemical mechanism underlying the T2D and AD interaction.

Table 1

Percent of Region with Aβ plaque

Brain region	**T2D-AD +/-**
Hippocampus	3.81%±0.16%*
Cortex	1.68%±0.13%*
Thalamus	0.21%±0.04%*

A one-way repeated measures ANOVA with Tukey's HSD post-hoc test indicates the plaque distribution varies significantly between the hippocampus, cortex, and thalamus. Data are shown as mean ± SEM. The * mark denotes statistical difference with $p<0.05$.

Table 2
Barnes maze escape latencies

Day	T2D-AD -/-	T2D-AD +/-
2	89.0±0.6	90.0±0.0
3	84.1±2.0	88.4±1.1
4	83.7±2.0	89.3±0.8
5	76.1±2.8*	89.8±0.2
6	74.1±2.6*	89.6±0.4

Barnes maze escape latencies for T2D-AD rats for days 2-6 of testing. The * mark denotes statistical difference ($p < 0.05$) between the T2D-AD -/- vs T2D-AD +/- latencies.

Table 3
Barnes maze search strategies

Rat	Search strategy	Day 2	Day 3	Day 4	Day 5	Day 6
T2D-AD -/-	Direct	2%	14%	17%	38%	42%
	Random	87%	75%	74%	58%	53%
	Serial	11%	11%	9%	4%	5%
T2D-AD +/-	Direct	2%	10%	22%	9%	3%
	Random	93%	83%	75%	88%	85%
	Serial	5%	8%	3%	3%	12%

Barnes maze search strategies for T2D-AD rats in days 2-6 of testing. Data are shown as the percentage of trials where rats use direct, random, and serial search strategies.

Table 4

Body Weight of T2D-AD Rats

Age, mos	T2D-AD -/-	T2D-AD +/-
1	115±1	114±2
2	376±3	383±3
3	538±5	547±3
4	577±14	597±14
5*	636±9	577±15
6*	639±10	558±7
7*	599±21	529±12
8*	553±15	497±7
9*	577±16	513±8

Body weight (in grams) of T2D-AD rats from 1-9 mos of age. For T2D-AD -/- rats (n= 13-99) show a significant weight difference from the T2D-AD +/- rats (n=10-90) starting at month 5. Data are shown as mean ± SEM. The * mark denotes statistical difference with $p<0.05$.

Table 5
Glucose and Insulin Levels

	Fasting insulin, ng/mL		Fasting glucose, mg/dL		Non-fasting glucose mg/dL	
Months	**T2D-AD -/-**	**T2D-AD +/-**	**T2D-AD -/-**	**T2D-AD +/-**	**T2D-AD -/-**	**T2D-AD +/-**
-4.0		0.22±0.13				166±6
-3.0	0.11±0.04	0.43±0.14		99±3	166±5	182±6
-2.0	0.43±0.10	1.85±0.33	104±2	110±5	180±4	198±5
-1.0	1.92±0.34	4.42±0.34	113±5	110±5	204±5	357±9
0.0	3.84±0.42	1.66±0.23	117±6	211±24	281±5	511±9
1.0	4.01±0.28	0.68±0.09	111±5	314±26	394±11	561±12
2.0	1.22±0.38	0.49±0.06	183±18	399±13	457±21	581±8
3.0	0.82±0.28	0.37±0.13	282±27	463±23	475±22	
4.0	0.73±0.18		319±22			

Glucose and insulin levels of T2D-AD -/- and T2D-AD +/- rats. The diabetes onset references at 0 month when T2D-AD -/- rat non fasting glucose level exceeds 250 mg/dl. Data are shown as mean ± SEM

Table 6
Metabolite Distribution with [1-^{13}C] Pyruvate Precursor

Metabolite/tC	SD	T2D-AD -/-	T2D-AD +/-
Lac/tC	0.109±0.006	0.146±0.008	0.212±0.013
Ala/tC	0.051±0.004	0.076±0.008	0.078±0.004
Pyr/tC	0.774±0.008	0.715±0.017	0.661±0.011
Bic/tC	0.018±0.002	0.011±0.001	0.009±0.001
Ala/lac	0.479±0.064	0.522±0.054	0.381±0.040
Pyr/lac	7.161±0.468	5.016±0.351	3.211±0.262
Bic/Lac	0.164±0.012	0.075±0.005	0.042±0.004

Metabolite distribution, metabolite ratio, and relative metabolite production rate after the injection of hyperpolarized [1-^{13}C]-pyruvate in the control (n = 3), T2D-AD -/- (n = 8), and T2D-AD +/- (n = 7) rats. Data are shown as mean ± SEM.

ACKNOWLEDGMENTS

The authors would like to acknowledge funding support from the California Department of Public Health, Chronic Disease Control Branch, Alzheimer's Disease Program (18-10923) and the scientific assistance of the following people: **Histology**: Alexander Borowsky, Katelyn Bump, and Brittany Dugger. **Cognitive Performance Test**: Julianna Porter, Katelyn Nielsen, Xiaoyou Luo, Angela DeJesus, Julia DeJesus, Meera Kohli, Rosalinda Moreno, Angelica Michelle Bachman, and Matthew Matson **Insulin Testing, Glucose Testing, Genetics:** UC Davis Mouse Biology Program, Tom Glaser, John Voss, Maha Al-Habeeb, Kalina Bertera, Julia Lee, Grace Yang, Theresa Phi, Sophia Litueva, and Kimiya Danaei. **Antibodies:** Fein Institute. **Rats:** Robert M. Cohen and Rat Resource & Research Center, Tg344AD rat; Peter Havel, UCD_T2DM rat. **Breeding**: James Graham; **^{13}C NMR Coil:** Ronald Watkins; **Scientific Discussion:** Robert M. Cohen, David Borchelt, James Graham.

The findings and conclusions in this report are those of the author(s) and do not necessarily represent the views or opinions of the California Department of Public Health or the California Health and Human Services Agency.

Figure Captions

Figure 1
Agarose DNA gel electrophoresis following polymerase chain reaction (PCR) of PS1, PrP, and APP genes. The far-left lane contains the DNA ladder. Both the T2D-AD -/-, T2D-AD +/- rats exhibit the Prp band at 799 bp. Only the T2D-AD +/- rat displays the PS1 and APP bands of the AD genes at 1,300 and 400 bp, respectively.

Figure 2
Histology of 9 mos brain: A) T2D-AD -/- and B) T2D-AD +/- shows that T2D-AD -/- rat shows no sign of Aβ. Only T2D-AD +/- brain has Aβ.

Figure 3
Histogram of the positive areas of the Aβ plaque in different regions of 9 mos rat brain: A one-way repeated measures ANOVA with Tukey's HSD post-hoc test indicates the plaque distribution varies significantly between the hippocampus, cortex, and thalamus in T2D-AD +/- rats ($F_{2,12} = 235.45$, $p = 2.35\times10^{-10}$). It also confirms significant plaques difference between the hippocampus and the cortex ($p = 6.83\times10^{-8}$), the hippocampus and the thalamus ($p = 1.70\times10^{-10}$), and the cortex and the thalamus ($p = 3.80\times10^{-6}$). The * mark indicates statistical significance.

Figure 4
Barnes maze escape latencies for T2D-AD rats for days 2-6 of testing: A mixed two-way repeated-measures ANOVA, with strain (T2D-AD -/-, T2D-AD +/-) as the between-subjects factor and day (2-6) as the within-subjects factor shows significant difference with respect to strain ($F_{1,28} = 16.27$, $p = 3.84\times10^{-4}$), day ($F_{3,90} = 5.74$, $p = 9.60\times10^{-4}$), and strain × day ($F_{3,90} = 6.18$, $p = 5.58\times10^{-4}$) on the latencies of T2D-AD -/- and T2D-AD +/- rats. A two-tailed t-test assuming unequal variances with the Bonferroni correction indicates significant difference on day 5 ($t(14) = -3.26$, $p = 2.87\times10^{-2}$) and day 6 ($t(14) = -4.40$, $p = 3.02\times10^{-3}$). For T2D-AD -/- and T2D-AD +/- rats, n = 15. Data points are shown as mean ± standard error of the mean ± SEM. The * mark indicates statistical significance.

Figure 5
Barnes maze search strategies for T2D-AD rats (n=15) for days 2-6 of testing. Histograms show the percentage of trials the rats used direct, random, and serial search strategies: A) T2D-AD -/- and B) T2D-AD +/- rats. Chi-square analysis of collapsed data across all trials reveals a significant difference in the distribution of search patterns between T2D-AD -/- and T2D-AD +/- rats ($\chi^2 = 16.13$, $df = 2$, $p = 3.15\times10^{-4}$).

Figure 6
Body weight (in grams, g) of T2D-AD rats from 1-9 months of age: The weights range from 115-577g. A two-tailed t-test assuming unequal variances with Bonferroni's correction indicates significant differences in the body weights between T2D-AD -/- and T2D-AD +/- rats at mos 5 ($t(37) = 3.41$, $p = 1.72\times10^{-2}$). A two-tailed t-test assuming equal variances with Bonferroni's correction confirms at mos 7 ($t(25) = 3.15$, $p = 3.79\times10^{-2}$). The number of rats in a month used to create the body profile ranges from n=10-99. Data shown as mean ± SEM. The * mark indicates statistical significance.

Figure 7
Modified Kaplan-Meier analysis of diabetes incidence as determined from non-fasting glucose level >250 mg/dl: The log-rank tests reveal a significant difference in the 50% point of diabetes incidence in the T2D-AD -/- (solid line) and T2D-AD +/- (dotted line) rats (χ^2(df = 1, n = 192) = 23.21, p = 1.45×10^{-6}). Surviving rats developed diabetes (T2D-AD -/-, 91.9% (91/99); T2D-AD +/-, 96.8% (90/93)). A significant difference in the age of diabetes onset appeared in the T2D-AD -/- and T2D-AD +/- rats (t(151) = 5.41, p = 2.46×10^{-7}). The T2D-AD +/- rat displays an average age of diabetes onset about a month earlier than the T2D-AD -/- rat.

Figure 8
Non-fasting blood glucose of T2D-AD -/- rats (solid line) and T2D-AD +/- rats (dashed line) before and after the onset of diabetes referenced to the T2D-AD -/- rat diabetes onset as 0: A two-tailed t-test assuming unequal variances with the Bonferroni correction indicates a significant difference in the glucose level of the 2 rat models at the age of onset of diabetes of the T2D-AD -/- rat at 0 mos (t(133) = -23.24, p = 8.12×10^{-48}). At the age of onset of diabetes for the T2D-AD +/- rats a similar significant difference in the glucose level occurs (t(132) = -15.20, p = 5.98×10^{-30}). For T2D-AD -/- rats, n = 36, 58, 68, 52, 42, 23, and 12, respectively. For T2D-AD +/- n = 11, 50, 81, 88, 91, 28, and 12, respectively. Linear regressions of the data at -1, 0, and 1 months for the T2D-AD -/- and the T2D-AD +/- rats show non-fasting glucose level rising at 95 mg/dL/month (R^2 = 0.98) and 156 mg/dL/month (R^2 = 0.99). Data points are shown as mean ± SEM.

Figure 9
Fasting blood glucose of T2D-AD -/- rats (solid line) and T2D-AD +/- rats (dashed line) before and after the onset of diabetes referenced to the T2D-AD -/- rat diabetes onset as 0: A two-tailed t-test assuming unequal variances with the Bonferroni correction indicates significant difference in the glucose level of the 2 rat models starting at the age of onset of diabetes of the T2D-AD -/- rat at 0 mos (t(17) = -3.84, p = 9.09×10^{-3}). For T2D-AD -/- rats, n = 10, 21,17, 13, 12, 14, and 7, respectively. For T2D-AD +/- rats, n = 10, 25, 21, 16, 16, 19, and 8, respectively. Linear regressions of the data at 0, 1, 2, 3, and 4 months shows fasting glucose levels of the T2D-AD -/- and T2D-AD +/- rats rising at 57 mg/dL/month (R^2 = 0.92) and 89 mg/dL/month (R^2 = 0.99), respectively. Data points are shown as mean ± SEM.

Figure 10
Fasting insulin concentrations of the T2D-AD -/- rats (solid line) and T2D-AD +/- rats (dashed line) before and after the onset of diabetes referenced to the diabetes onset of the T2D-AD -/- rat as 0: A two-tailed t-test assuming equal variances with the Bonferroni correction indicates significant differences in the insulin level of the 2 rat models at the age of onset of diabetes of the T2D-AD -/- rat at 0 mos (t(14) = 4.59, p = 3.39×10^{-3}) and at the age of onset of diabetes of the T2D-AD +/- rat at -1 mos (t(18) = -5.19, p = 4.96×10^{-4}). For T2D-AD -/- rats, -3, -2, -1, 0, 1, 2, 3, and 4 months before and after the age of onset of diabetes, n = 4, 7, 10, 8, 8, 4, 5, and 4, respectively. For T2D-AD +/- rats, the corresponding -3, -2, -1, 0, 1, 2, 3, and 4 months, n = 4, 7, 10, 10, 8, 8, 9, and 3, respectively Data points are shown as mean ± SEM.

Figure 11
A representative set of 2 min time averaged ^{13}C spectra after injection of hyperpolarized [1-^{13}C]-pyruvate: A) Control, B) T2D-AD -/-, and C) T2D-AD +/-. Spectra show signals corresponding to lactate, pyruvate-hydrate, alanine, pyruvate, and bicarbonate.

Figure 12
Histogram of bic/lac ratio in control, T2D-AD -/-, and T2D-AD +/- rat brains: A one-way between subjects ANOVA indicates the bic/lac ratio varies significantly between the control, T2D-AD -/-, and T2D-AD +/- rats ($F_{2,15} = 84.04$, $p = 7.09\times10^{-9}$). Tukey's HSD test indicates that the bic/lac ratio differs significantly between the control and the T2D-AD -/- rats ($p = 2.42\times10^{-7}$), the control and the T2D-AD +/- rats ($p = 4.34\times10^{-9}$), and the T2D-AD -/- and the T2D-AD +/- rats ($p = 7.75\times10^{-4}$). Data are shown as mean ± SEM. The * mark indicates statistical significance.

DECLARATIONS

Funding

The study acknowledges funding support from the California Department of Public Health 18-10923 (TJ).

Conflict of Interest

The authors declare no conflict of interest.

Contribution Statement

TJ, UR, KD, SCL, QC, HM, RB, RH, DS contributed to the conception and design of research; TJ, UR, KD, SCL, JMP, RS, DH, VT, QC, HM performed experiments; TJ, UR, KD, SCL, JMP, QC, HM, RS, DH, VT, RB, RH, and DS discussed, analyzed, and interpreted experiment data; TJ, UR, and KD prepared figures; TJ, UR wrote the drafts of the manuscript and incorporated comments; TJ, UR reviewed and approved the final version of the manuscript.

Availability of data and material

All data generated or analyzed during this study are included in this published article.

Ethics approval

Animal care and experimental procedures followed the guidelines of the National Institute of Health Office for Laboratory Animal Welfare and were approved by the local Institutional Animal Care and Use Committee

References

1. Arvanitakis Z, Wilson RS, Bienias JL, Evans DA & Bennett DA (2004) Diabetes mellitus and risk of Alzheimer disease and decline in cognitive function. ArchNeurol 61:661-666

2. Craft S (2009) The role of metabolic disorders in Alzheimer disease and vascular dementia: two roads converged. ArchNeurol 66:300-305

3. Craft S, Newcomer J, Kanne S, Dagogo-Jack S, Cryer P, Sheline Y, Luby J, Dagogo-Jack A & Alderson A (1996) Memory improvement following induced hyperinsulinemia in Alzheimer's disease. NeurobiolAging 17:123-130

4. Craft S, Peskind E, Schwartz MW, Schellenberg GD, Raskind M & Porte D, Jr. (1998) Cerebrospinal fluid and plasma insulin levels in Alzheimer's disease: relationship to severity of dementia and apolipoprotein E genotype. Neurology 50:164-168

5. Leibson CL, Rocca WA, Hanson VA, Cha R, Kokmen E, O'Brien PC & Palumbo PJ (1997) Risk of dementia among persons with diabetes mellitus: a population-based cohort study. AmJEpidemiol 145:301-308

6. Ott A, Stolk RP, Hofman A, van Harskamp F, Grobbee DE & Breteler MM (1996) Association of diabetes mellitus and dementia: the Rotterdam Study. Diabetologia 39:1392-1397

7. DeFronzo RA (2009) Banting Lecture. From the triumvirate to the ominous octet: a new paradigm for the treatment of type 2 diabetes mellitus. Diabetes 58:773-795

8. Banks WA (2012) Brain meets body: the blood-brain barrier as an endocrine interface. Endocrinology 153:4111-4119

9. Dienel GA & Hertz L (2001) Glucose and lactate metabolism during brain activation. JNeurosciRes 66:824-838

10. Hopkins DF & Williams G (1997) Insulin receptors are widely distributed in human brain and bind human and porcine insulin with equal affinity. DiabetMed 14:1044-1050

11. Rodin J, Wack J, Ferrannini E & DeFronzo RA (1985) Effect of insulin and glucose on feeding behavior. Metabolism 34:826-831

12. Schulingkamp RJ, Pagano TC, Hung D & Raffa RB (2000) Insulin receptors and insulin action in the brain: review and clinical implications. NeurosciBiobehavRev 24:855-872

13. Gray SM, Meijer RI & Barrett EJ (2014) Insulin regulates brain function, but how does it get there? Diabetes 63:3992-3997 https://doi.org/10.2337/db14-0340

14. Vandal M, White PJ, Chevrier G, Tremblay C, St-Amour I, Planel E, Marette A & Calon F (2015) Age-dependent impairment of glucose tolerance in the 3xTg-AD mouse model of Alzheimer's disease. FASEB J 29:4273-4284 https://doi.org/10.1096/fj.14-268482

15. Takeda S, Sato N, Uchio-Yamada K, Sawada K, Kunieda T, Takeuchi D, Kurinami H, Shinohara M, Rakugi H & Morishita R (2010) Diabetes-accelerated memory dysfunction via cerebrovascular

inflammation and Abeta deposition in an Alzheimer mouse model with diabetes. Proc Natl Acad Sci U S A 107:7036-7041 https://doi.org/10.1073/pnas.1000645107

16. Games D, Buttini M, Kobayashi D, Schenk D & Seubert P (2006) Mice as models: transgenic approaches and Alzheimer's disease. J Alzheimers Dis 9:133-149 https://doi.org/10.3233/jad-2006-9s316

17. Hsiao K, Chapman P, Nilsen S, Eckman C, Harigaya Y, Younkin S, Yang F & Cole G (1996) Correlative memory deficits, Abeta elevation, and amyloid plaques in transgenic mice. Science 274:99-102

18. Quon D, Wang Y, Catalano R, Scardina JM, Murakami K & Cordell B (1991) Formation of beta-amyloid protein deposits in brains of transgenic mice. Nature 352:239-241 https://doi.org/10.1038/352239a0

19. Cohen RM, Rezai-Zadeh K, Weitz TM, Rentsendorj A, Gate D, Spivak I, Bholat Y, Vasilevko V, Glabe CG, Breunig JJ, et al. (2013) A transgenic Alzheimer rat with plaques, tau pathology, behavioral impairment, oligomeric abeta, and frank neuronal loss. J Neurosci 33:6245-6256 https://doi.org/10.1523/JNEUROSCI.3672-12.2013

20. Hallam TM, Floyd CL, Folkerts MM, Lee LL, Gong QZ, Lyeth BG, Muizelaar JP & Berman RF (2004) Comparison of behavioral deficits and acute neuronal degeneration in rat lateral fluid percussion and weight-drop brain injury models. J Neurotrauma 21:521-539 https://doi.org/10.1089/089771504774129865

21. Hanes J, Zilka N, Bartkova M, Caletkova M, Dobrota D & Novak M (2009) Rat tau proteome consists of six tau isoforms: implication for animal models of human tauopathies. J Neurochem 108:1167-1176 https://doi.org/10.1111/j.1471-4159.2009.05869.x

22. Loeffler DA (2004) Using animal models to determine the significance of complement activation in Alzheimer's disease. J Neuroinflammation 1:18 https://doi.org/10.1186/1742-2094-1-18

23. Mullins JJ, Peters J & Ganten D (1990) Fulminant hypertension in transgenic rats harbouring the mouse Ren-2 gene. Nature 344:541-544 https://doi.org/10.1038/344541a0

24. Herrera VL, Makrides SC, Xie HX, Adari H, Krauss RM, Ryan US & Ruiz-Opazo N (1999) Spontaneous combined hyperlipidemia, coronary heart disease and decreased survival in Dahl salt-sensitive hypertensive rats transgenic for human cholesteryl ester transfer protein. Nat Med 5:1383-1389 https://doi.org/10.1038/70956

25. Cummings BP, Digitale EK, Stanhope KL, Graham JL, Baskin DG, Reed BJ, Sweet IR, Griffen SC & Havel PJ (2008) Development and characterization of a novel rat model of type 2 diabetes mellitus: the UC Davis type 2 diabetes mellitus UCD-T2DM rat. AmJPhysiol RegulIntegrComp Physiol 295:R1782-R1793

26. Park JM, Josan S, Hurd RE, Graham J, Havel PJ, Bendahan D, Mayer D, Chung Y, Spielman DM & Jue T (2021) Hyperpolarized NMR study of the impact of pyruvate dehydrogenase kinase inhibition on the pyruvate dehydrogenase and TCA flux in type 2 diabetic rat muscle. Pflugers Archiv : European journal of physiology https://doi.org/10.1007/s00424-021-02613-3

27. Park JM, Josan S, Mayer D, Hurd RE, Chung Y, Bendahan D, Spielman DM & Jue T (2015) Hyperpolarized 13C NMR observation of lactate kinetics in skeletal muscle. J Exp Biol 218:3308-3318 https://doi.org/10.1242/jeb.123141

28. Hwang JJ, Bini J & Belfort-DeAguiar R (2025) Measurement of brain glucose metabolism in obesity and diabetes. Diabetologia 68:1879-1888 https://doi.org/10.1007/s00125-025-06491-7

29. Choi YS, Kang S, Ko SY, Lee S, Kim JY, Lee H, Song JE, Kim DH, Kim E, Kim CH, et al. (2018) Hyperpolarized [1-13C] pyruvate MR spectroscopy detect altered glycolysis in the brain of a cognitively impaired mouse model fed high-fat diet. Mol Brain 11:74 https://doi.org/10.1186/s13041-018-0415-2

30. Chen Z & Zhong C (2013) Decoding Alzheimer's disease from perturbed cerebral glucose metabolism: implications for diagnostic and therapeutic strategies. Prog Neurobiol 108:21-43 https://doi.org/10.1016/j.pneurobio.2013.06.004

31. Moreira PI, Santos MS, Moreno AM, Seica R & Oliveira CR (2003) Increased vulnerability of brain mitochondria in diabetic (Goto-Kakizaki) rats with aging and amyloid-beta exposure. Diabetes 52:1449-1456 https://doi.org/10.2337/diabetes.52.6.1449

32. Hoppener JW & Lips CJ (2006) Role of islet amyloid in type 2 diabetes mellitus. Int J Biochem Cell Biol 38:726-736 https://doi.org/10.1016/j.biocel.2005.12.009

33. Jankowsky JL, Slunt HH, Ratovitski T, Jenkins NA, Copeland NG & Borchelt DR (2001) Co-expression of multiple transgenes in mouse CNS: a comparison of strategies. Biomol Eng 17:157-165 https://doi.org/10.1016/s1389-0344(01)00067-3

34. Chen JQ, Mori H, Cardiff RD, Trott JF, Hovey RC, Hubbard NE, Engelberg JA, Tepper CG, Willis BJ, Khan IH, et al. (2015) Abnormal Mammary Development in 129:STAT1-Null Mice is Stroma-Dependent. PLoS One 10:e0129895 https://doi.org/10.1371/journal.pone.0129895

35. Fedor M, Berman RF, Muizelaar JP & Lyeth BG (2010) Hippocampal theta dysfunction after lateral fluid percussion injury. J Neurotrauma 27:1605-1615 https://doi.org/10.1089/neu.2010.1370

36. Fox GB, Fan L, LeVasseur RA & Faden AI (1998) Effect of traumatic brain injury on mouse spatial and nonspatial learning in the Barnes circular maze. J Neurotrauma 15:1037-1046 https://doi.org/10.1089/neu.1998.15.1037

37. Ardisson LP, Minicucci MF, Azevedo PS, Chiuso-Minicucci F, Matsubara BB, Matsubara LS, Santos PP, Assalin HB, Novo R, Novelli EL, et al. (2012) Influence of AIN-93 diet on mortality and cardiac remodeling after myocardial infarction in rats. Int J Cardiol 156:265-269 https://doi.org/10.1016/j.ijcard.2010.10.128

38. Bikman BT, Guan Y, Shui G, Siddique MM, Holland WL, Kim JY, Fabrias G, Wenk MR & Summers SA (2012) Fenretinide prevents lipid-induced insulin resistance by blocking ceramide biosynthesis. J Biol Chem 287:17426-17437 https://doi.org/10.1074/jbc.M112.359950

39. Price TO, Eranki V, Banks WA, Ercal N & Shah GN (2012) Topiramate treatment protects blood-brain barrier pericytes from hyperglycemia-induced oxidative damage in diabetic mice. Endocrinology 153:362-372 https://doi.org/10.1210/en.2011-1638

40. Baena-Nieto G, Lomas-Romero IM, Mateos RM, Leal-Cosme N, Perez-Arana G, Aguilar-Diosdado M, Segundo C & Lechuga-Sancho AM (2017) Ghrelin mitigates beta-cell mass loss during insulitis in an animal model of autoimmune diabetes mellitus, the BioBreeding/Worcester rat. Diabetes Metab Res Rev 33https://doi.org/10.1002/dmrr.2813

41. Visser J, Groen H, Klatter F & Rozing J (2002) Timing of pentoxifylline treatment determines its protective effect on diabetes development in the Bio Breeding rat. Eur J Pharmacol 445:133-140 https://doi.org/10.1016/s0014-2999(02)01625-4

42. Mody N, Agouni A, McIlroy GD, Platt B & Delibegovic M (2011) Susceptibility to diet-induced obesity and glucose intolerance in the APP (SWE)/PSEN1 (A246E) mouse model of Alzheimer's disease is associated with increased brain levels of protein tyrosine phosphatase 1B (PTP1B) and retinol-binding protein 4 (RBP4), and basal phosphorylation of S6 ribosomal protein. Diabetologia 54:2143-2151 https://doi.org/10.1007/s00125-011-2160-2

43. Lutz TA & Meyer U (2015) Amylin at the interface between metabolic and neurodegenerative disorders. Frontiers in neuroscience 9:216 https://doi.org/10.3389/fnins.2015.00216

44. Baloyannis SJ (2006) Mitochondrial alterations in Alzheimer's disease. JAlzheimersDis 9:119-126

45. Sims NR (1996) Energy metabolism, oxidative stress and neuronal degeneration in Alzheimer's disease. Neurodegeneration 5:435-440

46. Fukuyama H, Ogawa M, Yamauchi H, Yamaguchi S, Kimura J, Yonekura Y & Konishi J (1994) Altered cerebral energy metabolism in Alzheimer's disease: a PET study. Journal of nuclear medicine : official publication, Society of Nuclear Medicine 35:1-6

47. Craft S, Raman R, Chow TW, Rafii MS, Sun CK, Rissman RA, Donohue MC, Brewer JB, Jenkins C, Harless K, et al. (2020) Safety, Efficacy, and Feasibility of Intranasal Insulin for the Treatment of Mild Cognitive Impairment and Alzheimer Disease Dementia: A Randomized Clinical Trial. JAMA Neurol 77:1099-1109 https://doi.org/10.1001/jamaneurol.2020.1840

48. Long C, Han X, Yang Y, Li T, Zhou Q & Chen Q (2022) Efficacy of intranasal insulin in improving cognition in mild cognitive impairment or dementia: a systematic review and meta-analysis. Front Aging Neurosci 14:963933 https://doi.org/10.3389/fnagi.2022.963933

49. Egefjord L, Gejl M, Moller A, Braendgaard H, Gottrup H, Antropova O, Moller N, Poulsen HE, Gjedde A, Brock B, et al. (2012) Effects of liraglutide on neurodegeneration, blood flow and cognition in Alzheimer s disease - protocol for a controlled, randomized double-blinded trial. Dan Med J 59:A4519

50. McClean PL & Holscher C (2014) Liraglutide can reverse memory impairment, synaptic loss and reduce plaque load in aged APP/PS1 mice, a model of Alzheimer's disease. Neuropharmacology 76 Pt A:57-67 https://doi.org/10.1016/j.neuropharm.2013.08.005

51. Talbot K (2014) Brain insulin resistance in Alzheimer's disease and its potential treatment with GLP-1 analogs. Neurodegener Dis Manag 4:31-40 https://doi.org/10.2217/nmt.13.73

52. Agrawal R, Zhuang Y, Cummings BP, Stanhope KL, Graham JL, Havel PJ & Gomez-Pinilla F (2014) Deterioration of plasticity and metabolic homeostasis in the brain of the UCD-T2DM rat model of naturally occurring type-2 diabetes. Biochim Biophys Acta 1842:1313-1323 https://doi.org/10.1016/j.bbadis.2014.05.007

53. Aubert A, Costalat R, Magistretti PJ & Pellerin L (2005) Brain lactate kinetics: Modeling evidence for neuronal lactate uptake upon activation. Proc Natl Acad Sci U S A 102:16448-16453

54. Aubert A, Pellerin L, Magistretti PJ & Costalat R (2007) A coherent neurobiological framework for functional neuroimaging provided by a model integrating compartmentalized energy metabolism. Proc Natl Acad Sci U S A 104:4188-4193

55. Pellerin L & Magistretti PJ (1994) Glutamate uptake into astrocytes stimulates aerobic glycolysis: a mechanism coupling neuronal activity to glucose utilization. Proc Natl Acad Sci U S A 91:10625-10629

56. Shulman RG, Hyder F & Rothman DL (2001) Cerebral energetics and the glycogen shunt: neurochemical basis of functional imaging. Proc NatlAcadSci USA 98:6417-6422

57. Boumezbeur F, Mason GF, de Graaf RA, Behar KL, Cline GW, Shulman GI, Rothman DL & Petersen KF (2010) Altered brain mitochondrial metabolism in healthy aging as assessed by in vivo magnetic resonance spectroscopy. J Cereb Blood Flow Metab 30:211-221

58. Shulman GI, Rothman DL, Jue T, Stein P, DeFronzo RA & Shulman RG (1990) Quantitation of muscle glycogen synthesis in normal subjects and subjects with non-insulin-dependent diabetes by 13C nuclear magnetic resonance spectroscopy. N Engl J Med 322:223-228 https://doi.org/10.1056/NEJM199001253220403

59. Ashleigh T, Swerdlow RH & Beal MF (2023) The role of mitochondrial dysfunction in Alzheimer's disease pathogenesis. Alzheimers Dement 19:333-342 https://doi.org/10.1002/alz.12683

60. Nasb M, Tao W & Chen N (2024) Alzheimer's Disease Puzzle: Delving into Pathogenesis Hypotheses. Aging Dis 15:43-73 https://doi.org/10.14336/AD.2023.0608

61. Rudman MD, Ulrich JD & Holtzman DM (2026) Recent advances in Alzheimer's disease: From molecular mechanisms to therapeutic strategies. Cell 189:4193-4224 https://doi.org/10.1016/j.cell.2026.06.006

62. Jensen NJ, Porse AJ, Wodschow HZ, Speyer H, Krogh J, Marner L, Gejl M, Gjedde A & Rungby J (2025) Relation of Insulin Resistance to Brain Glucose Metabolism in Fasting and Hyperinsulinemic States: A Systematic Review and Meta-analysis. J Clin Endocrinol Metab 110:e525-e537 https://doi.org/10.1210/clinem/dgae570

63. Swerdlow RH (2023) The Alzheimer's Disease Mitochondrial Cascade Hypothesis: A Current Overview. J Alzheimers Dis 92:751-768 https://doi.org/10.3233/JAD-221286

64. Tang S, Liao Y, Yang M & Yue R (2026) Brain insulin resistance: a key pathological hub linking metabolic and neuropsychiatric comorbidities. Front Aging Neurosci 18:1716291 https://doi.org/10.3389/fnagi.2026.1716291

65. Wei Y, Du X, Guo H, Han J & Liu M (2024) Mitochondrial dysfunction and Alzheimer's disease: pathogenesis of mitochondrial transfer. Front Aging Neurosci 16:1517965 https://doi.org/10.3389/fnagi.2024.1517965

66. Leibold N, Bain JR & Despa F (2024) Type-2 Diabetes, Pancreatic Amylin, and Neuronal Metabolic Remodeling in Alzheimer's Disease. Mol Nutr Food Res 68:e2200405 https://doi.org/10.1002/mnfr.202200405

67. Reutzel M, Grewal R, Joppe A & Eckert GP (2022) Age-Dependent Alterations of Cognition, Mitochondrial Function, and Beta-Amyloid Deposition in a Murine Model of Alzheimer's Disease-A Longitudinal Study. Front Aging Neurosci 14:875989 https://doi.org/10.3389/fnagi.2022.875989

Figure 1

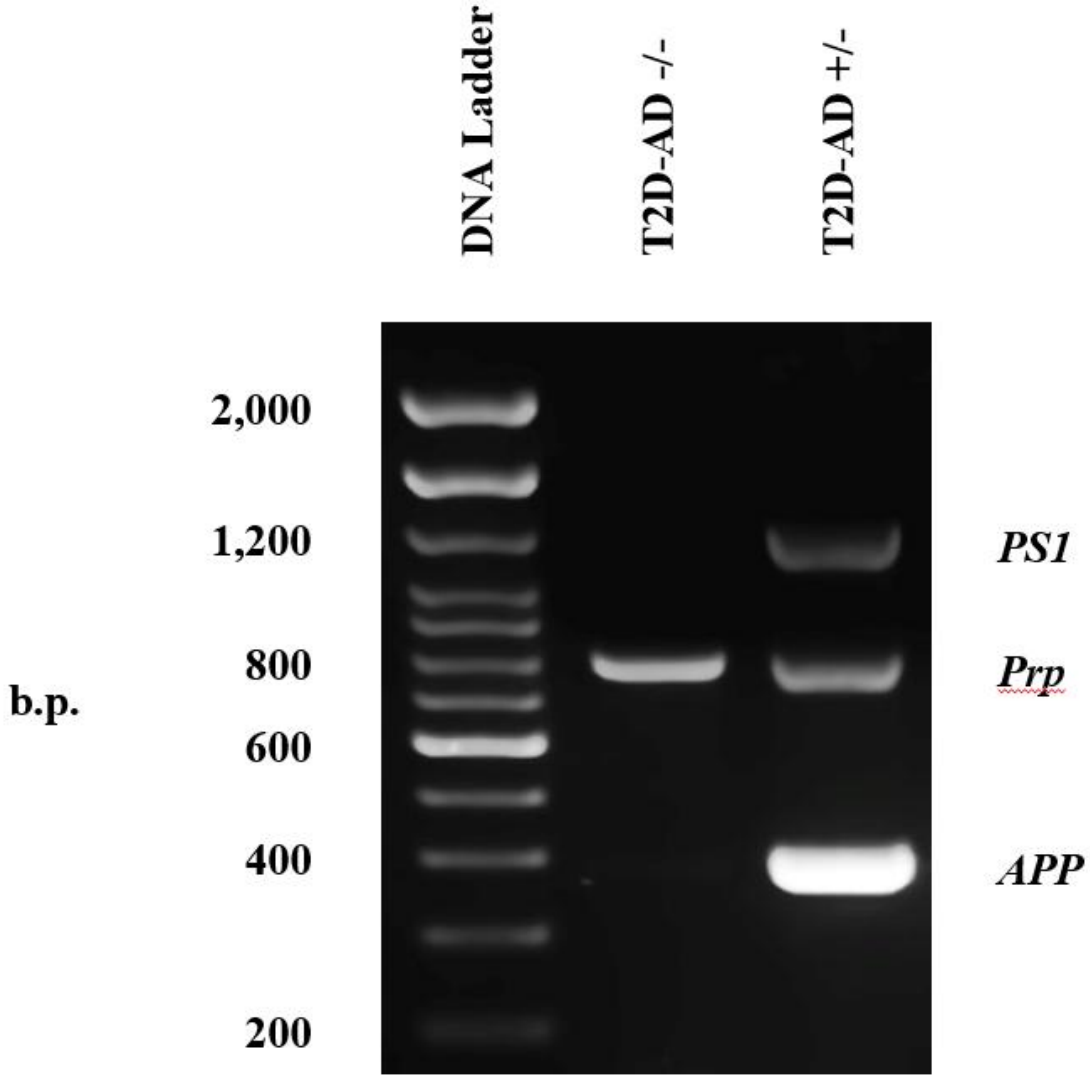
DNA Ladder
T2D-AD -/-
T2D-AD +/-
2,000
1,200
800
600
400
200
b.p.
PS1
Prp
APP

Figure 2

A

B

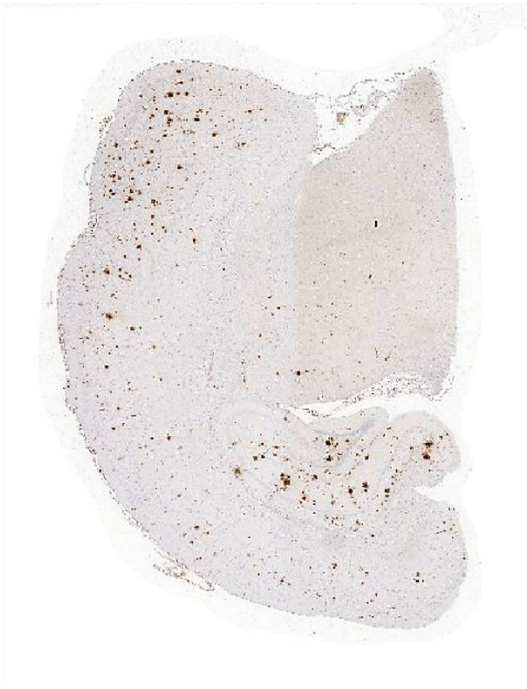

Figure 3

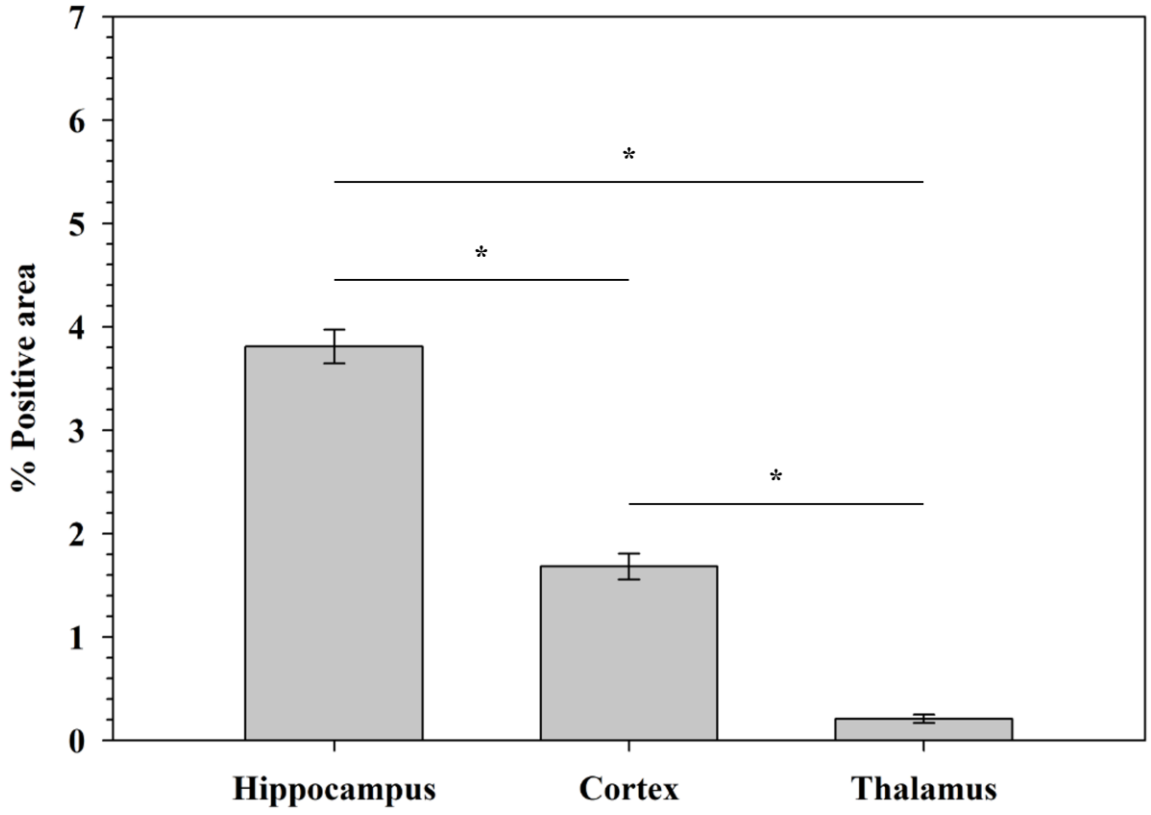

Figure 4

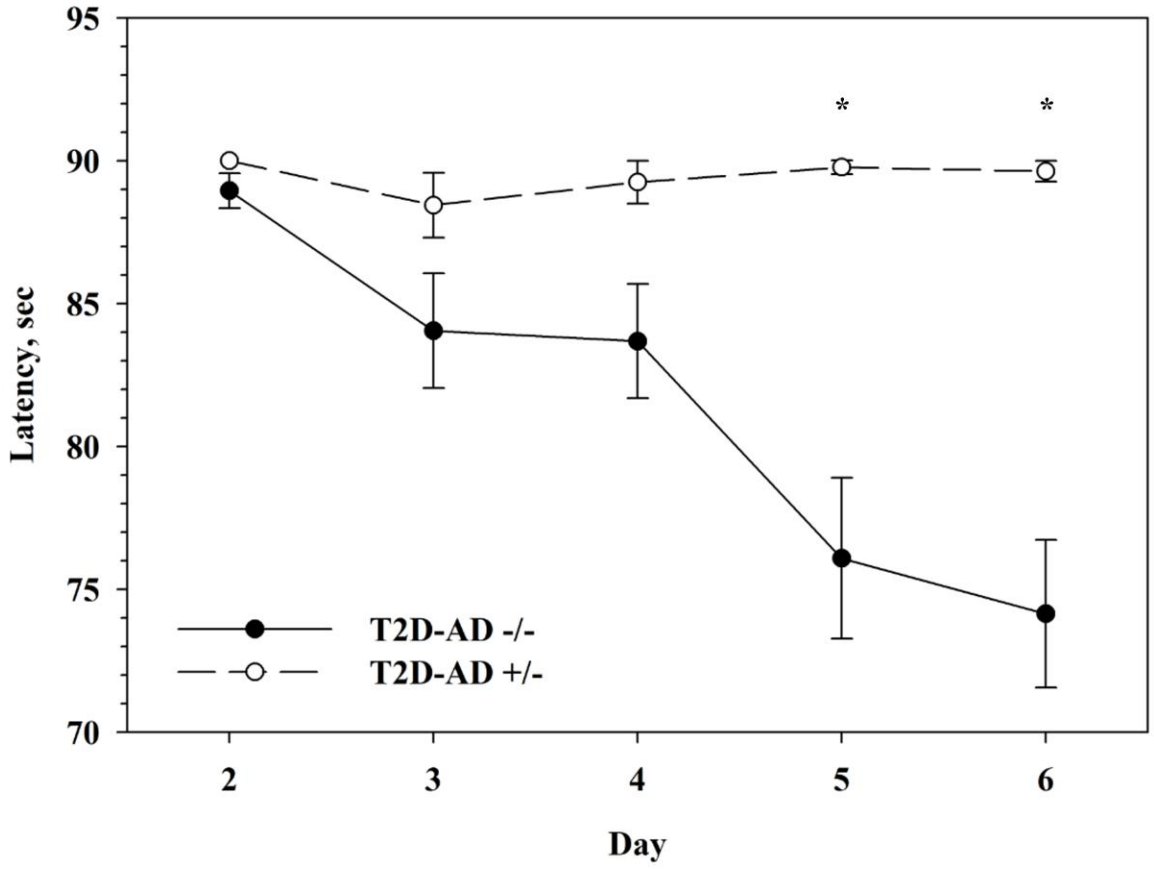

Figure 5

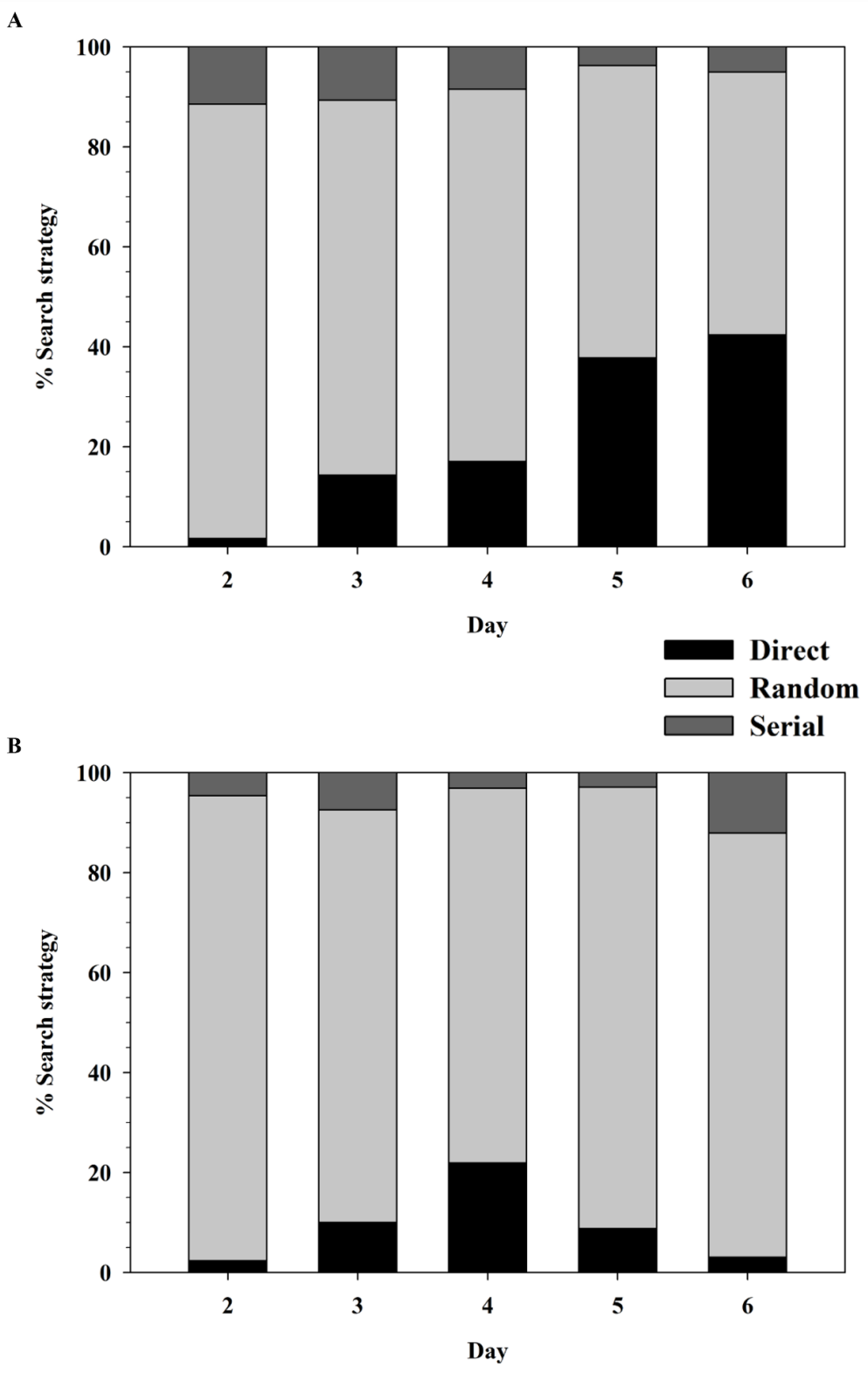
A
100
80
60
40
20
0
% Search strategy
2
3
4
5
6
Day
Direct
Random
Serial
B
100
80
60
40
20
0
% Search strategy
2
3
4
5
6
Day

Figure 6

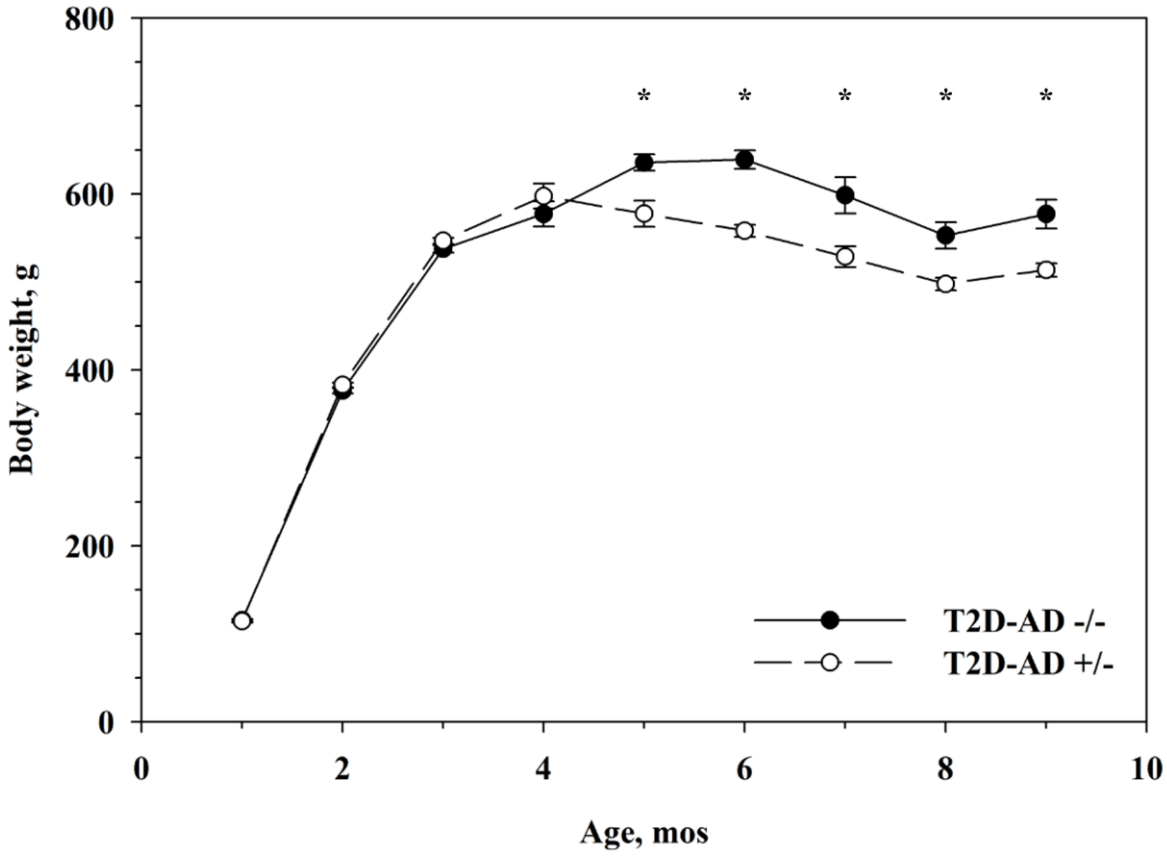

Figure 7

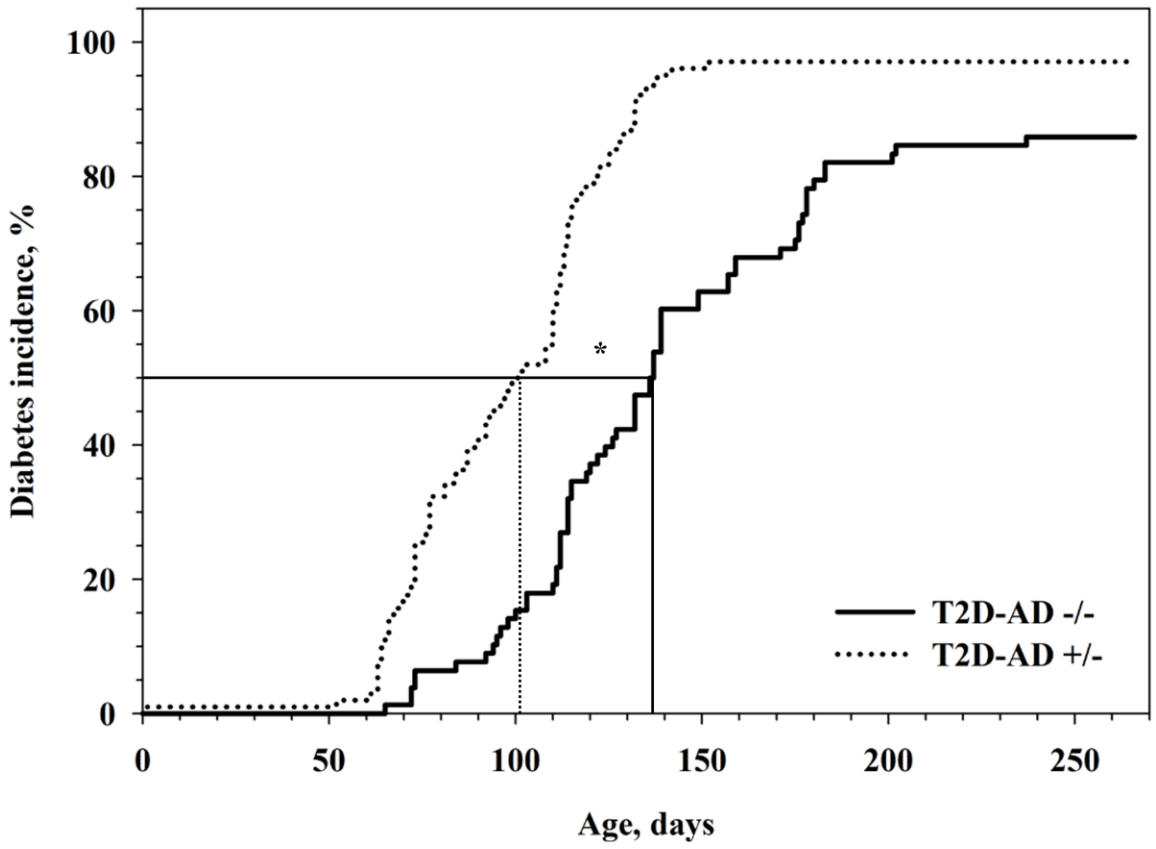
Diabetes incidence, %
100
80
60
40
20
0
0
50
100
150
200
250
Age, days
*
T2D-AD -/-
T2D-AD +/-

Figure 8

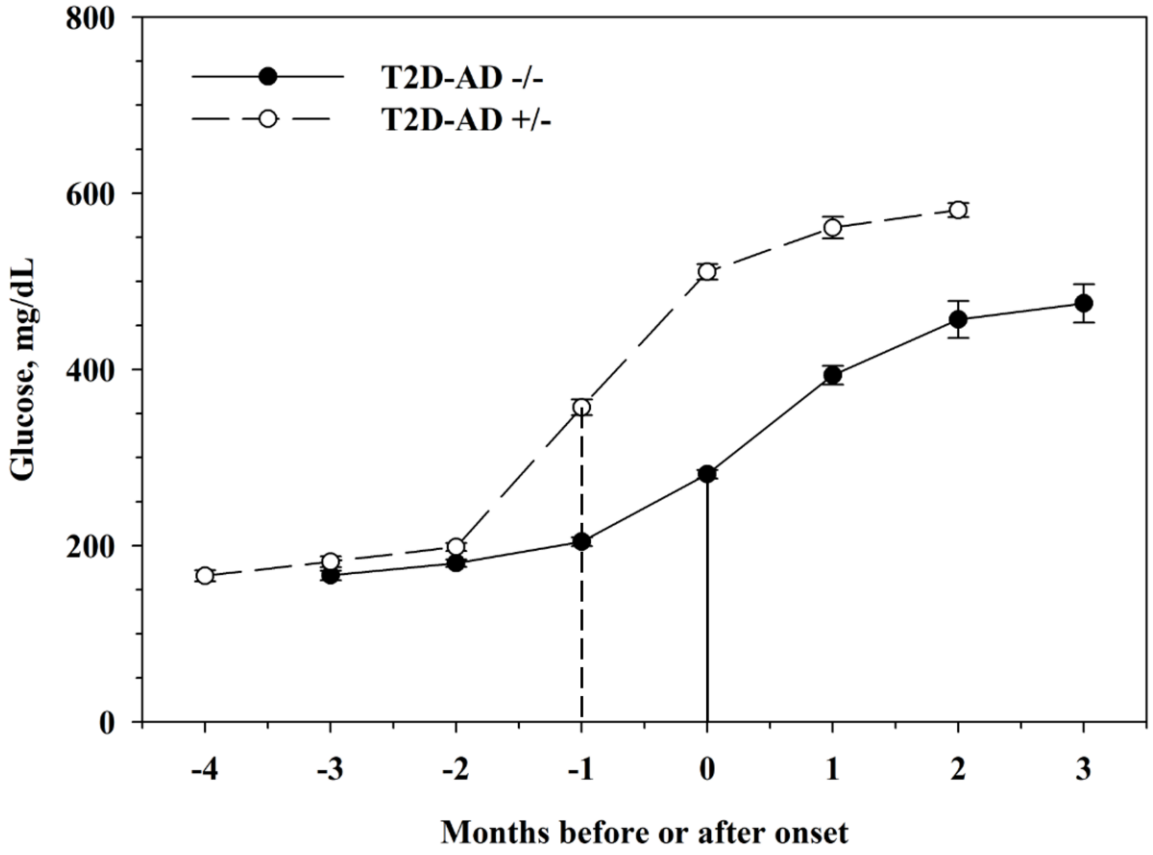
800
600
400
200
0
Glucose, mg/dL
T2D-AD -/-
T2D-AD +/-
-4
-3
-2
-1
0
1
2
3
Months before or after onset

Figure 9

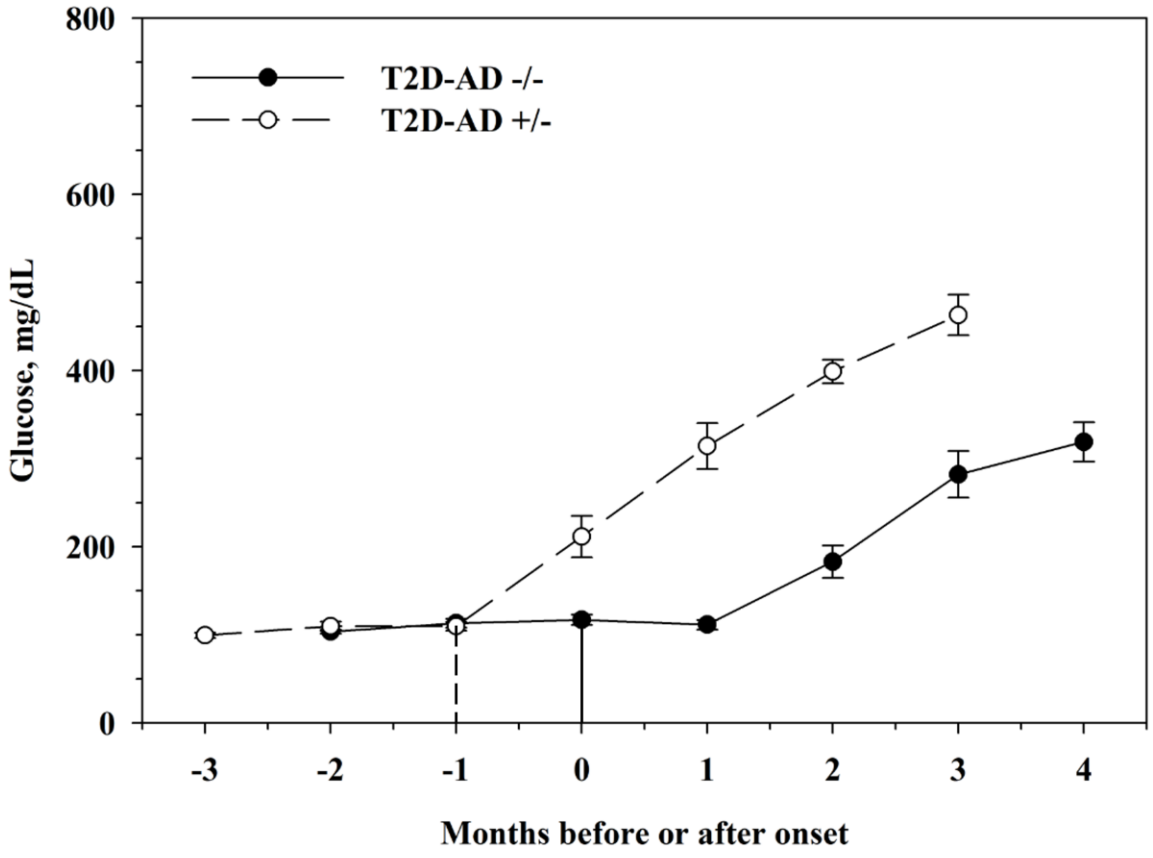
800
600
400
200
0
Glucose, mg/dL
T2D-AD -/-
T2D-AD +/-
-3
-2
-1
0
1
2
3
4
Months before or after onset

Figure 10

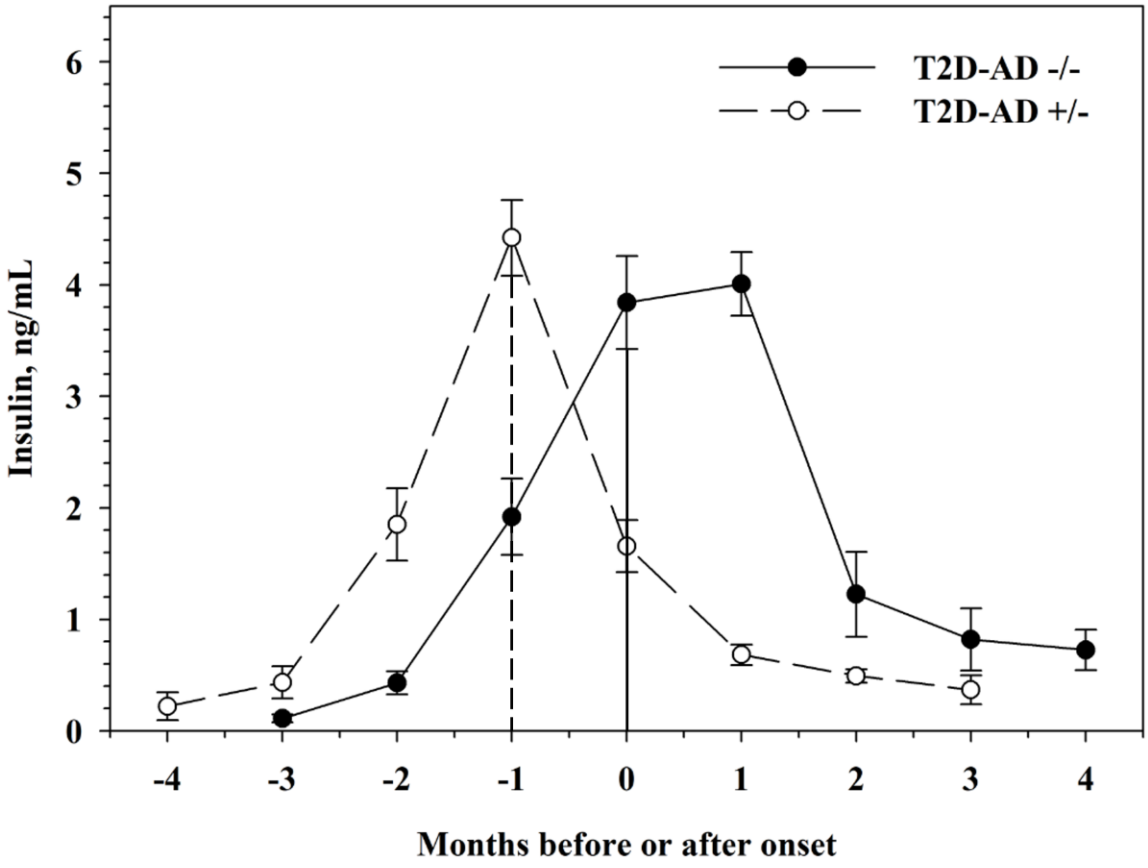
T2D-AD -/-
T2D-AD +/-
Insulin, ng/mL
0
1
2
3
4
5
6
-4
-3
-2
-1
0
1
2
3
4
Months before or after onset

Figure 11

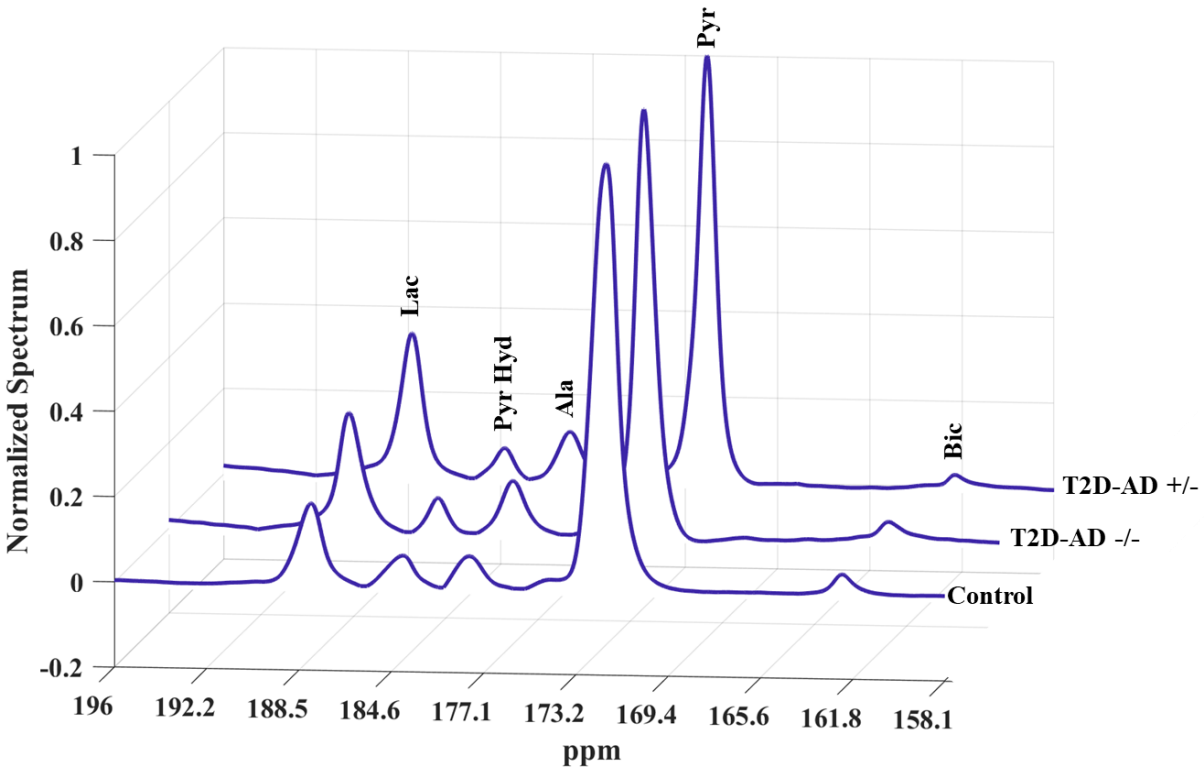
Pyr
Lac
Pyr Hyd
Ala
Bic
T2D-AD +/-
T2D-AD -/-
Control
Normalized Spectrum
1
0.8
0.6
0.4
0.2
0
-0.2
196
192.2
188.5
184.6
177.1
173.2
169.4
165.6
161.8
158.1
ppm

Figure 12